Journal of Medicinal Chemistry

Article

Structure–activity relationships of cyclo(L-tyrosyl-L-tyrosine) derivatives binding to Mycobacterium tuberculosis CYP121: iodinated analogues promote shift to high-spin adduct

Sunnia Rajput, Kirsty J. McLean, Harshwardhan Poddar, Irwin Selvam, Gayathri Nagalingam, James A Triccas, Colin Levy, Andrew W. Munro, and Craig A Hutton

J. Med. Chem., **Just Accepted Manuscript** • DOI: 10.1021/acs.jmedchem.9b01199 • Publication Date (Web): 16 Oct 2019

Structure–activity relationships of cyclo(L-tyrosyl-L-tyrosine) derivatives binding to *Mycobacterium tuberculosis* CYP121: iodinated analogues promote shift to high-spin adduct

Sunnia Rajput,[†] Kirsty J. McLean,[‡] Harshwardhan Poddar,[‡] Irwin R. Selvam,[‡] Gayathri Nagalingam,[¶] James A. Triccas,[¶] Colin W. Levy,[‡] Andrew W. Munro[‡] and Craig A. Hutton[*,†]*

[†] School of Chemistry and Bio21 Molecular Science and Biotechnology Institute, University of Melbourne, 30 Flemington Rd, Parkville, VIC 3010, Australia

[‡] Centre for Synthetic Biology of Fine and Specialty Chemicals (SYNBIOCHEM), Manchester Institute of Biotechnology, School of Chemistry, University of Manchester, 131 Princess Street, Manchester M1 7DN, U.K.

[¶] Department of Infectious Diseases and Immunology, Sydney Medical School, The University of Sydney, Sydney, NSW 2006, Australia

chutton@unimelb.edu.au

ABSTRACT:

A series of analogues of cyclo(L-tyrosyl-L-tyrosine), the substrate of the *Mycobacterium tuberculosis* enzyme CYP121, have been synthesized and analyzed by UV-Vis and EPR spectroscopy and by X-ray crystallography. The introduction of iodine substituents onto cyclo(L-tyrosyl-L-tyrosine) results in sub-μM binding affinity for the CYP121 enzyme and a complete shift to the high spin state of the heme Fe^{III}. The introduction of halogens that are able to interact with heme groups is thus a feasible approach to the development of next-generation, tight binding inhibitors of the CYP121 enzyme, in the search for novel anti-tubercular compounds.

INTRODUCTION

The successful development of effective antimicrobial agents has largely focused on the elucidation and targeting of biosynthetic pathways that are not present in humans.[1-3] This approach has been validated through numerous examples, including antibiotics that target the bacterial cell wall (e.g. β-lactams and vancomycin) and essential bacterial enzymes (e.g. sulfonamide drugs). The knowledge necessary for the development of such antimicrobial agents includes a detailed understanding of the molecular mechanisms of the enzymes present in such microbial biosynthetic pathways.

The sequencing of the genome of *Mycobacterium tuberculosis* (Mtb)[4-6] has unveiled several essential genes from this pathogen that presumably encode for essential proteins. Amongst these essential genes is one that encodes an unusual cytochrome P450 enzyme (CYP) known as CYP121A1 (referred to as CYP121 hereafter).[7] While most CYPs oxidize substrates through incorporation of an oxygen atom,[8] CYP121 catalyzes the oxidative coupling of two tyrosine residues in the substrate cyclodityrosine (cYY, **1**) to generate a C–C bond, forming the product mycocyclosin **2** (Scheme 1).[9] This CYP-catalyzed oxidative coupling is closely related to the processes involved in biosynthesis of glycopeptide antibiotics such as vancomycin and teicoplanin.[10] CYP121 is not found in other microorganisms, nor humans, and is therefore a valid target for development of specific agents against Mtb. In order to initiate such development, much knowledge needs to be uncovered about this unusual enzyme.

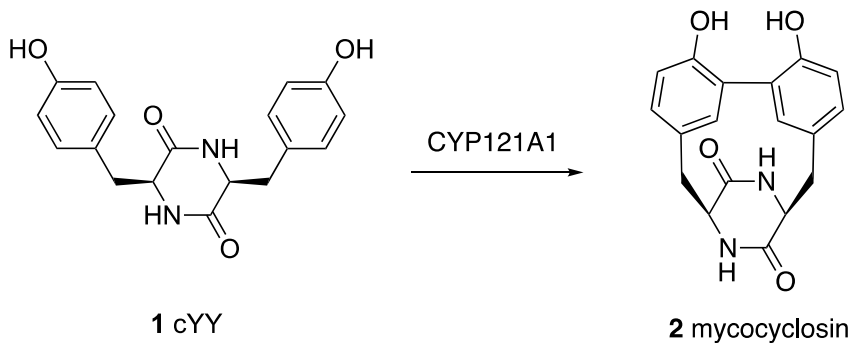

1 cYY **2** mycocyclosin

Scheme 1: CYP121 catalyzed biosynthesis of mycocyclosin **2** from cyclo(Tyr-Tyr) (cYY, **1**).

CYP121 has been shown to bind tightly to azole antifungal drugs, suggesting this enzyme is a possible target of such drugs.[11,12] Azole drugs are known to affect antimicrobial activity through inhibition of CYPs, though they are not highly selective for different CYP isoforms.[11,13] Belin et al. determined the substrate of CYP121 to be cyclodityrosine **1**,[9] and demonstrated that the enzyme catalyzes oxidative C–C bond formation to generate mycocyclosin **2**. The essential nature of the gene encoding the CYP121 enzyme suggests mycocyclosin has a unique role in Mtb biology, which has yet to be determined. Diketopiperazines (DKPs, cyclic dipeptides) such as cyclodityrosine **1** are common secondary metabolites.[14] However, oxidative coupling to generate side-chain cross-links in such systems is highly unusual. The few structurally related natural products that have been reported are the herqulines[15-20] and piperazinomycin.[21-23] The unusual chemical process catalyzed by CYP121 and the unusual structural features of mycocyclosin[24,25] suggest that selective inhibitors of this enzyme can be developed towards the search for novel anti-tubercular therapies.

Preliminary structure-activity relationships have been reported by Belin and coworkers,[26] who showed the CYP121 can bind closely related substrate analogues including cYF and cYW with comparable affinities to the natural substrate, but that these analogues do not exhibit significant catalytic turnover. Only minor modifications to the substrate were tolerated with more significant

variations to the substrate structure, including loss of one of the aromatic side chains, change in stereochemistry or 'ring opening' to acyclic dipeptides, resulting in greatly diminished or complete loss of binding affinity.

Small N-heterocycles have been discovered to bind to CYP121 with reasonable affinity.[27-31] Several iterations of fragment-based discovery and intuitive design by Abell and co-workers have unveiled the highest affinity compounds to date; anilinophenylpyrazoles which possess nM affinity for CYP121 (K_D = 15 nM).[31]

The extent of the structure–activity relationships of DKP-type substrate analogues has to date been limited to readily accessible compounds prepared from commercially available amino acid starting materials. We sought to probe structure–activity relationships of a wider range of substrate analogues and to further define the binding requirements of CYP121 as an important step toward developing potent inhibitors of this enzyme.

Design of substrate analogues

We describe herein the design and synthesis of a range of cYY analogues to further probe structure–activity relationships of CYP121 binding compounds. Modifications at the 4-position of the aromatic ring have been designed to interrogate the role of the tyrosyl phenolic groups on the binding affinity to CYP121. Analogues that lack one or both phenolic groups (**3**, **4**), or have one or both phenolic groups blocked with *O*-methyl groups (**5**, **6**), have been designed. Further, the phenolic groups have been replaced with halogens (**7**, **8**). Halogen (**9**–**14**) and methyl substituents (**15**–**18**) have been introduced at positions *ortho*- or *meta*- to the phenols on the tyrosyl aromatic rings, to probe the steric and electronic effects on binding to CYP121 (Figure 1).

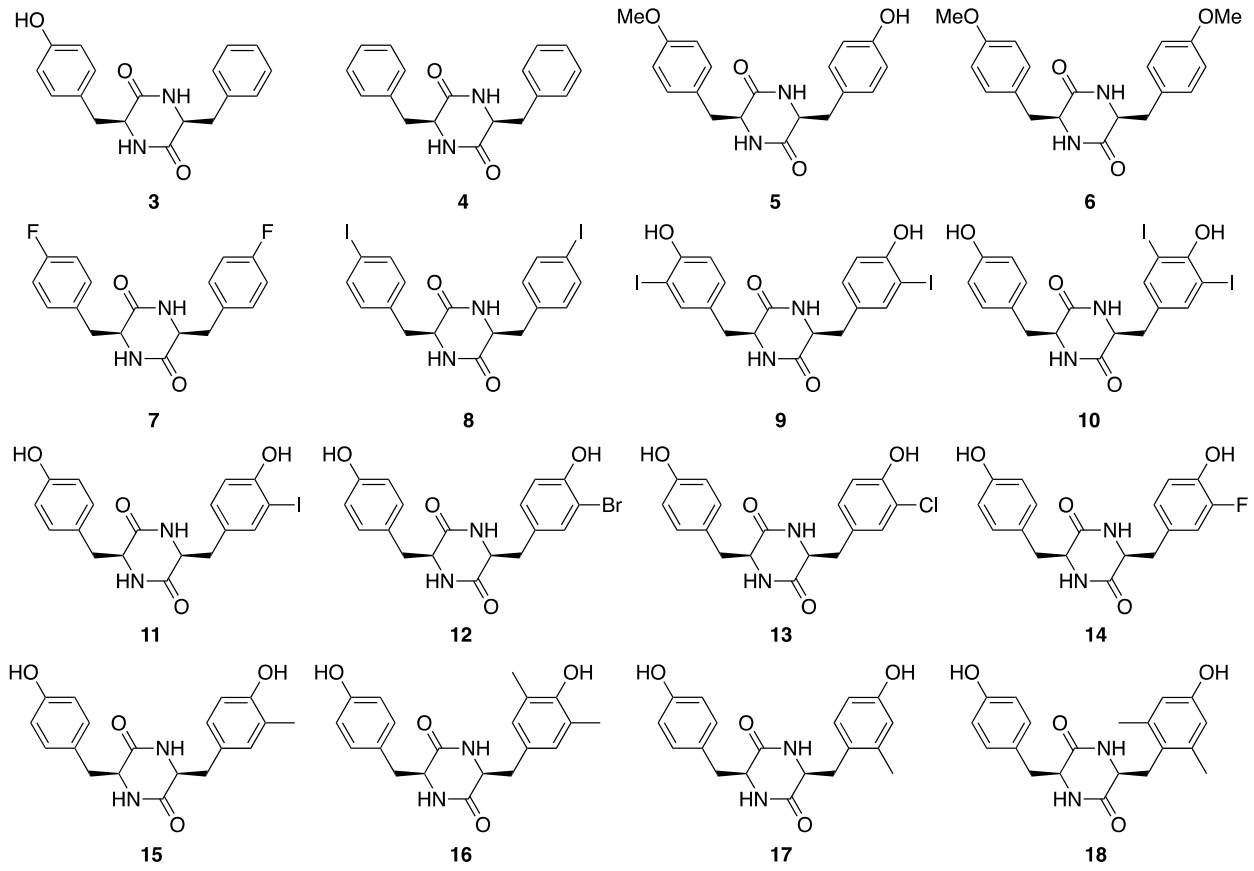

Figure 1: Designed substrate analogues

RESULTS

Synthesis of substrate analogues

The synthesis of the substrate analogues **3**, **4**, **7**–**14** was conducted through a standard dipeptide cyclization route (Scheme 2).[24] N-Boc amino acids **19** were treated with an appropriate □-amino methyl ester **20**, *N,N,N′,N′*-tetramethyl-*O*-(1*H*-benzotriazol-1-yl)uronium hexafluorophosphate (HBTU, 1.1 equiv.) and *N*-hydroxybenzotriazole (HOBt, 1.1 equiv.) in DMF/acetonitrile to generate the corresponding dipeptides **21** in high yields (87–96%). The dipeptides were treated with excess formic acid to remove the Boc group, then cyclization was effected by heating in a mixture of toluene and *sec*-butanol to obtain the corresponding diketopiperazines (**3**, **4**, **7**–**14**).

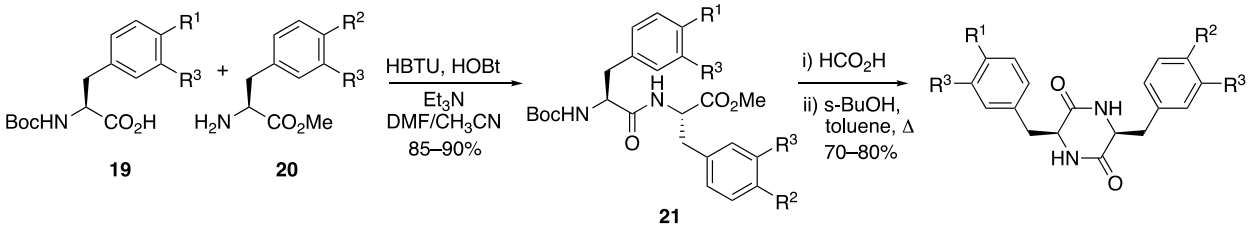

Scheme 2: Synthesis of diketopiperazines **3**–**6**, **9**–**14.**

Synthesis of the 4-*O*-methyl analogues **5** and **6** was performed at the dipeptide stage due to the difficulties associated with the purification of diketopiperazines, which mainly emanate from their highly insoluble nature. Thus, the tyrosyl–tyrosine dipeptide **21a** was treated with methyl iodide in the presence of anhydrous potassium carbonate to afford a mixture of doubly and singly methylated dipeptides **21b** and **21c** in 60% and 30% yield, respectively (Scheme 3). The dipeptides **21b** and **21c** were converted to diketopiperazines **5** and **6** following the general procedure described previously. The mono-methylated dipeptide **21b** was isolated as a 1:1 mixture of regioisomers, which were not separated as both isomers converge to the same diketopiperazine **5** after cyclization.

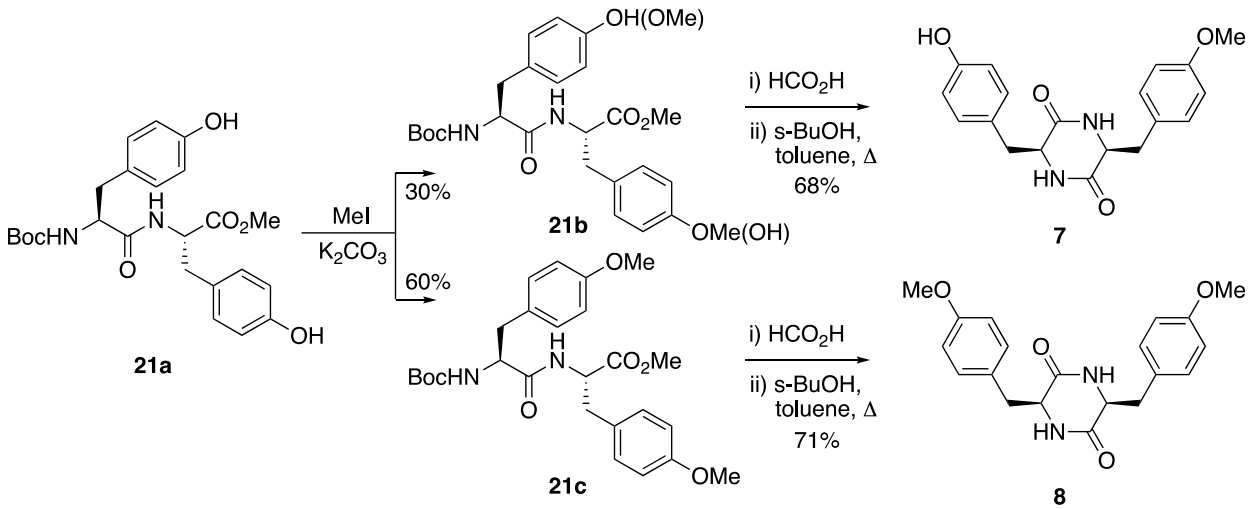

Scheme 3: Synthesis of methylated analogues **5** and **6**.

As the tyrosine derivatives containing methyl substituents at the 2- and 3-positions of the aromatic ring are not readily commercially available, a different route to compounds **15**–**18** was required. These analogues were generated via a Knoevenagal-type condensation reaction of triacetyl tyrosyl–glycine DKP **23** with substituted benzaldehydes **24** (Scheme 4).[32-34] Hydrogenation of the olefins **25** proceeds stereoselectively to generate the L,L-DKPs, with concomitant hydrogenolysis of the *O*-benzyl protecting groups. Olefins **25a**–**c** were susceptible to hydrogenation at 6 bar in the presence of Pd/C over 16–24 hours. Subsequent deacetylation with aqueous ammonia furnished cYY analogues **15**–**17**. The 2,6-dimethyl olefin **25d** required a higher pressure (30 bar) to effect reduction, presumably due to increased steric hindrance. Under these more forcing conditions, deacetylation of the intermediate occurred spontaneously to give **18** directly.

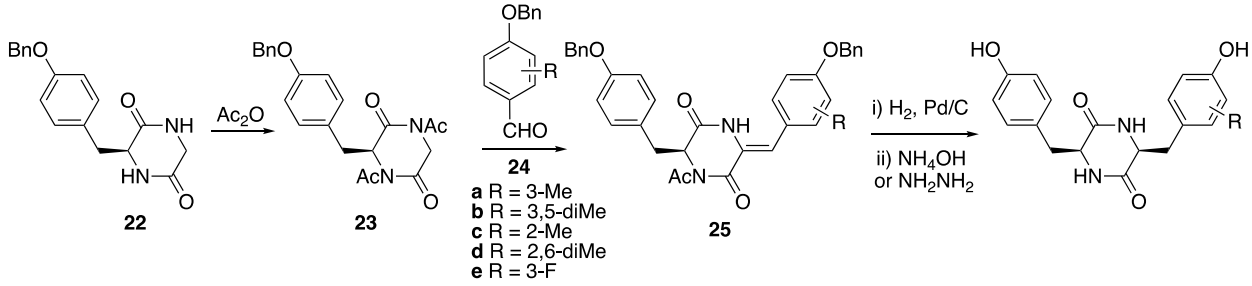

Scheme 4: Synthesis of DKPs **14**–**18** via Knoevenagel condensation/reduction.

The 3-fluoro analogue **14** could be prepared via this route (from 4-benzyloxy-3-fluorobenzaldehyde **24e**) using milder hydrogenation conditions (4–5 bar for 6 hours). However, preparation of the other halogenated derivatives **11**–**13** was not possible due to dehalogenation during the hydrogenation process.

Determination of binding affinities of substrate analogues to CYP121

Interactions of the natural substrate cYY **1** and analogues **3**–**18** with CYP121 were analyzed by UV-Visible spectroscopy. The ligands were titrated from 0 μM to the point where saturation of the signal was observed; i.e. there was no further change in absorbance. Typically, a decrease in the intensity of the Soret peak at 416 nm (associated with the Fe^{III} low spin state) is observed together with an increase in the intensity of the Soret peak at ~390 nm (associated with the Fe^{III} high spin state) as the concentration of the ligand is increased (Figure 2). All analogues displayed a blue shift of the Soret band (from 416 nm to ~390 nm) indicative of substrate-like or type-I binding.[35] The change in absorbance was plotted against ligand concentration to generate hyperbolic curves (Figure 3 and Figures S1–17) from which K_D values were derived (except for difluoro-analogue **5**, which exhibited a sigmoidal curve that was fitted to the Hill function, Fig.S6). The K_D values for ligands **3**–**18** are listed in Table 1. Even at saturating concentrations of substrate **1** and most substrate analogues, it was observed that there is a significant amount of enzyme remaining in the low spin state (e.g. Figure 2A). However, iodinated compounds **9** and **11**, and *O*-Me analogue **5**, resulted in a complete shift of the Soret band to the lower wavelength, high-spin state (e.g. Figure 2B).

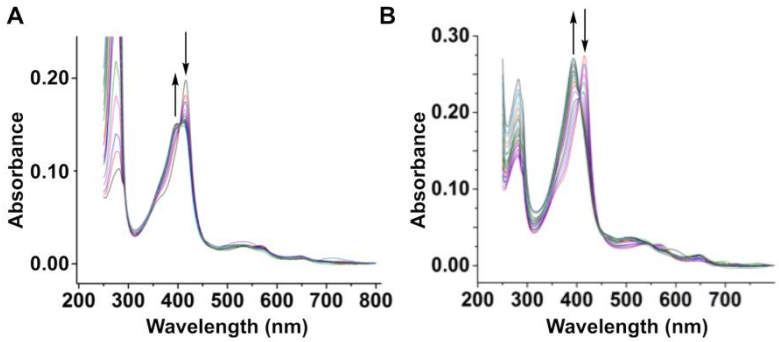

Figure 2: UV-visible spectrophotometric titration of CYP121 with the natural substrate **1** (A) and the 3-iodo-analogue **9** (B).

For the natural substrate cYY **1**, the K_D was determined to be 30±2 μM, which is in reasonable agreement with the previously reported value of 19.4 μM.[9] cYF **3** exhibited a K_D = 80.8±5.8 μM, in reasonable accordance with the reported K_D value.[26]

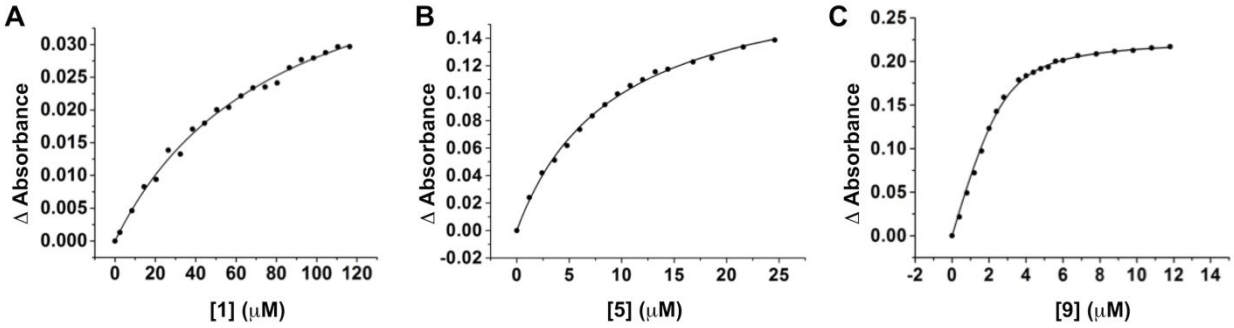

Figure 3: Plots of change in ligand-induced absorbance versus [ligand] for representative examples of (**A**) weak (**3**), (**B**) moderate (**5**) and (**C**) tight-binding (**9**) analogues.

Table 1: K_D values and percentage HS for binding of substrate **1** and analogues **3**–**18** to CYP121.

Compound	K_D (μM)	% HS	Compound	K_D (μM)	% HS
1	30 ± 2	52	**11**	0.28 ± 0.02	98
3	80.8 ± 5.8	5	**12**	0.46 ± 0.02	85
4	2.4 ± 0.1	3	**13**	1.5 ± 0.1	68
5	10.4 ± 0.5	61	**14**	12.8 ± 0.6	36
6	29.4 ± 1.1	35	**15**	1.1 ± 0.1	91
7	6.3 ± 0.3	1	**16**	15.1 ± 0.3	75
8	0.72 ± 0.1	3	**17**	39.8 ± 1.5	20
9	0.45 ± 0.04	100	**18**	> 100	1

10	9.1 ± 0.1	74

Introduction of one 'blocked' or methylated phenolic group (**5**) resulted in a three-fold increase in binding affinity (K_D = 10.4 μM) relative to cYY **1** (**(**K_D = 30 μM). Introduction of the second *O*-Me group (**6**) returned the binding affinity to a value similar to **1** (**(**K_D = 29 μM). Intriguingly, these results are the opposite of those observed where the phenols are removed rather than replaced: cYF **3** lacking one phenol has a decreased affinity for CYP121 (K_D = 80.8 μM), whereas cFF **4** lacking both phenols has a considerably increased binding affinity (K_D = 2.4 μM) (Table 1).

Replacement of the phenols with halogens (I or F, **7** and **8**) resulted in an increase in binding affinity. The fluorine-containing analogue **7** displayed a K_D = 6.3 μM, between that of the natural substrate cYY **1** and the cFF analogue **3**, though it displayed a sigmoidal rather than hyperbolic binding curve (Fig. S6). The iodine-containing analogue displayed an increased binding affinity (K_D = 0.7 μM).

Introduction of halogen substituents at position-3 resulted in increased binding affinity for CYP121. Binding affinity increased with increasing size of the halogen; F<Cl<Br<I (Table 1, **11**–**14**). As the iodinated analogues **8** and **11** exhibited sub-□M affinities, we investigated the effect of additional iodine substitution. Analogue **9** possessing 3-iodo substituents on both aromatic rings displayed similar binding affinity to **11** (K_D = 0.45 □M *cf.* 0.28 □M), suggesting the second iodine did not significantly affect affinity. Analogue **10** possessing a 3,5-diiodinated aromatic ring displayed reduced affinity relative to **11** (K_D = 9.1 □M *cf.* 0.28 □M), though still improved compared to cYY **1**.

The 3-methylated analogue **15** displayed an increased binding affinity (K_D = 1.1 μM) relative to cYY **1**, though not as great as the equivalent 3-iodo analogue **11**. Introduction of a second methyl

group in the form of the 3,5-dimethyl analogue reduced affinity (K_D = 15.1 μM), showing an effect similar to the 3,5-diiodo analogue **10**. The 2-methylated analogue **17** displayed slightly decreased binding affinity (K_D = 40 μM) relative to cYY **1**. The 2,6-dimethyl analogue, however, exhibited no binding to CYP121 (K_D >>100 μM), with no change observed in the UV-Vis spectrum even at 120 μM (Figure S17A).

EPR studies

The binding interactions of **1** and **3**–**18** were analyzed using EPR spectroscopy. EPR spectroscopy is extensively used in studies of CYP heme environment, ligand binding mode and oxidation state, and can provide an in-depth insight into the ligand–porphyrin interactions affecting the entire heme environment, particularly in the absence of further structural data. The EPR spectrum for substrate-free CYP121 shows a typical rhombic trio of g-tensor elements, observed for low spin heme iron.[7]

The EPR spectrum of CYP121 bound to the natural substrate **1** is shown in Figure 4B. The native CYP121 enzyme is almost completely low-spin, with negligible high-spin content. The g-values, together with an estimate of the amount of high spin complex observed, for substrate-free CYP121 and CYP121 bound to **1**, **3**–**18** are shown in Table 2.

Table 2: Summary of EPR analysis for CYP121 and in the presence of **1**, **3**–**18**[a]

Compd	g values (LS)	g values (HS)	~% HS	Compd	g values (LS)	g values (HS)	~% HS
–	2.49, 2.25, 1.88	–	0	**10**	2.45, 2.25, 1.90	8.04, 3.54, 1.68	38
1	2.46, 2.25, 1.90	8.05, 3.44, ND	2.7	**11**	2.46, 2.24, ND	7.98, 3.56, 1.68	86

3	2.45, 2.25, 1.90	8.05, 3.44, ND	1.4	**12**	2.46, 2.25, 1.90	8.06, 3.46, 1.66	68
4	2.49, 2.25, 1.88	–	0	**13**	2.46, 2.25, 1.90	7.98, 3.49, 1.67	21
5	2.45, 2.25, 1.90	8.00, 3.50, 1.66	64	**14**	2.46, 2.26, 1.89	7.96, 3.51, ND	1.2
6	2.47, 2.25, 1.89	7.96, 3.53, 1.68	56	**15**	2.46, 2.25, 1.90	8.01, 3.49, 1.66	11
7	2.49, 2.25, 1.88	7.8, ND, ND	1.5	**16**	2.46, 2.25, 1.90	8.05, 3.47,1.66	62
8	2.49, 2.25, 1.88	7.83, 3.64, ND	7.5	**17**	2.46, 2.25,1.90	8.01, 3.35, ND	0.6
9	–	7.96, 3.53, 1.68	100	**18**	2.47, 2.25, 1.89	7.94, 3.48, ND	1.9

[a] EPR spectra available in the SI (Figures S1–S17).

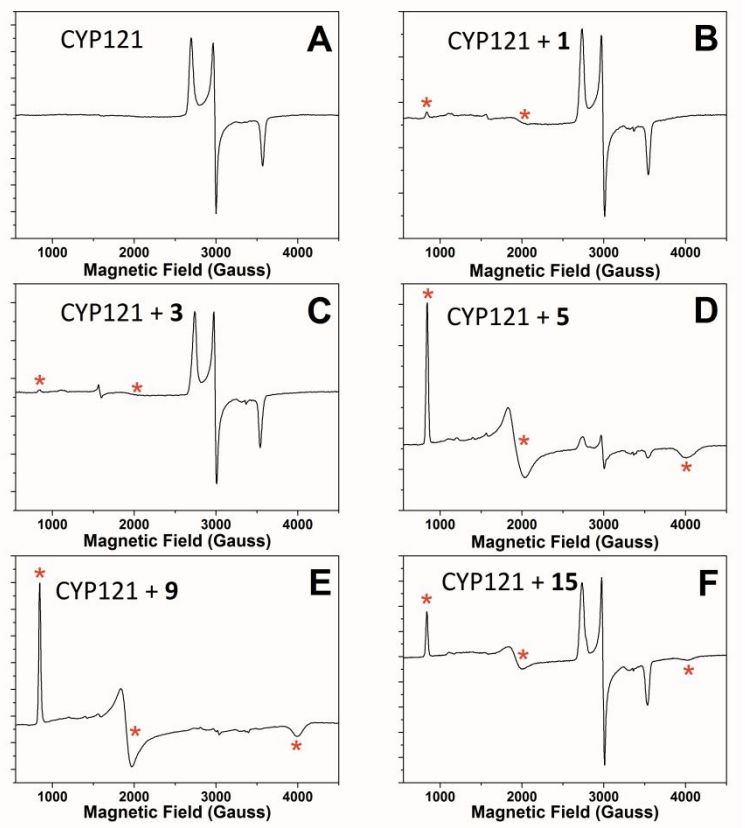

Figure 4: EPR spectra of CYP121 and with ligands **1**, **3**, **5**, **9** and **15** bound. (* = HS signal)

For cYF **3** ~1.4% high spin signal was observed (Figure 4C), while for cFF analogue **4** (Figure S3), no high spin signal was observed, despite improved binding affinity compared to cYF **3**. For the 4-F analogue **7** and the 4-I analogue **8**, the amount of high spin signal observed was comparable to the natural substrate **1**. Intriguingly, the EPR spectra for the mono- and bis-*O*-methyl analogues **5** and **6** showed much greater shift towards the high spin state (~64% and 56%, respectively, Figures 4D and S5). The 3-iodo analogues **9** and **11** induced an almost complete shift towards the high spin signal (Figures 4E and S10), indicative of tight binding with displacement of the H_2O ligand.

X-ray crystallography studies

X-ray crystal structures were obtained for CYP121 bound to **5**, **11** and **14**–**18**. The 3-methyl analogue with the substituted aromatic ring **15** (Figure 5A) binds within the enzyme active site. The 3-methyl substituent is bound efficiently in the CYP121 binding pocket of the enzyme active site distal to the heme, with no steric clashes or enzyme conformational changes observed. The binding of the ligand does not displace the water molecule associated with the Fe^{III} ion as the sixth ligand. The analogue **15** shows a direct hydrogen bonding interaction between the carbonyl group of the DKP ring and the side chain of the Asn85 residue. Other hydrogen bonding interactions to the ligand are formed through water molecules between the phenolic groups of the ligand and Thr77, Gln385 and Arg386 residues of the enzyme. There are also additional hydrophobic interactions between the 3-methyl substituent and the Phe168 and Val78 residues.

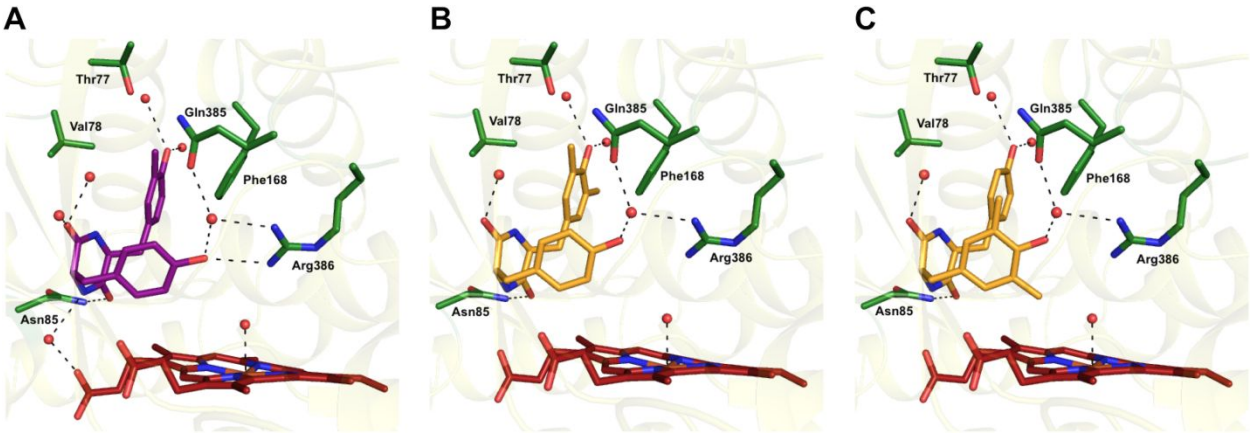

Figure 5: X-ray crystal structure of the 3-methyl analogue **15** and 3,5-dimethyl analogue **16** bound to CYP121 (PDB IDs 6RQ0, 6RQ5). The heme group is in red and the protein side chains in green. The red spheres denote water molecules. The dashed lines represent probable hydrogen bonds. (**A**); CYP with ligand **15** (purple). (**B**) and (**C**); two binding modes of CYP121 with ligand **16** (yellow).

The 3,5-dimethyl analogue **16** binds in two conformations: one conformation is similar to the 3-methyl analogue **15** (Figure 5B), while the second conformation is nearly perfectly overlaid with the first, but with the 3,5-dimethyl substituted aromatic ring orientated towards the heme (Figure 5C). The 3,5-dimethyl analogue **16** shows the same hydrogen bonding interactions with the residues Asn85, Thr77, Gln385 and Arg386 as observed for the analogue **15**. Further, similar van der Waals interactions between the 3-methyl substituent and Phe168/Val78 in the distal pocket are observed. However, the extra methyl substituent in each orientation buttresses against active site residues. In the first orientation, the 5-Me group is buttressed against the I helix, close to Val228, while in the second orientation, the 5-Me group forces the Gln385 side-chain to move away to accommodate the hydrophobic methyl group.

The 2,6-dimethyl analogue **18** (Figure 6A) binds within the enzyme active site in a flipped conformation compared to the 3- and 3,5-substituted analogues, **15** and **16**, with the DKP ring interacting with the water molecule bound to the heme Fe^{III} ion. The substituted aromatic ring of **18** binds in the distal pocket, orientated away from the heme moiety, while the unsubstituted phenolic group is situated in the space occupied by the DKP ring of the natural substrate **1**. Thus, the phenolic group on the non-methylated aromatic ring shows a hydrogen bonding interaction with the Asn85 residue and the DKP ring shows a hydrogen bonding interaction with the Arg386 residue – the reverse of the interactions observed for the 3-methylated analogues. The water-mediated hydrogen-bonding interaction from the carbonyl groups on the DKP ring to Thr77 and Gln385 is still observed for this flipped binding conformation of analogue **18**, and the phenolic group on the aromatic ring bound in the distal pocket retains similar hydrogen bonding interactions to those observed for the other analogues. Arg386 makes a direct hydrogen bond with the carbonyl group on the DKP ring which is pointing towards the heme group. An additional hydrogen bonding interaction is observed from the nitrogen of the DKP ring to a water molecule. This flipped conformation resembles the binding mode of the related TxtC–thaxtomin D enzyme–substrate complex reported by Challis.[36] TxtC catalyzes the double hydroxylation of the DKP substrate, thaxtomin, via two distinct binding modes.

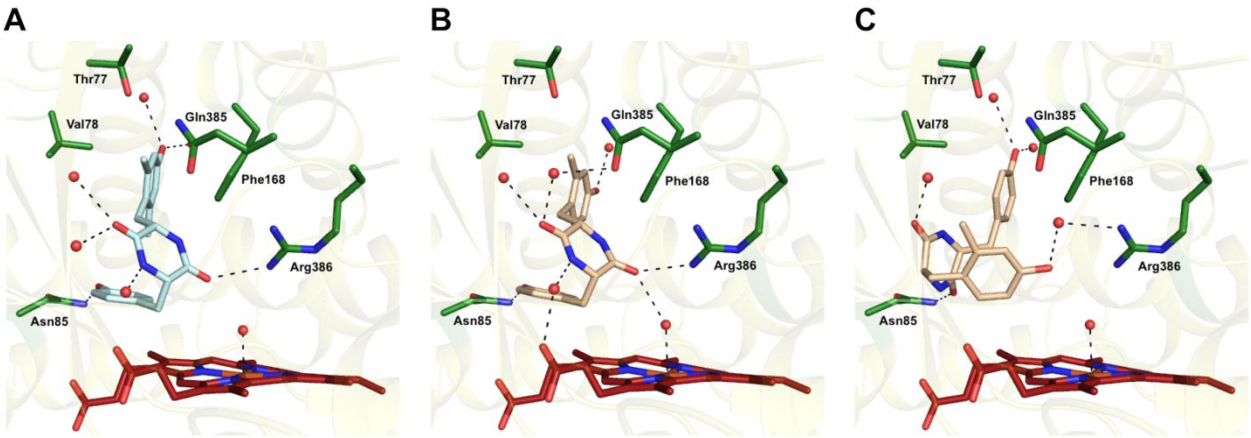

Figure 6: X-ray crystal structure of the 2-methyl analogue **17** and 2,6-dimethyl analogue **18** bound to CYP121 (PDB IDs 6RQ1, 6RQ3). The heme group is in red and the protein side chains are in green. The red spheres denote the water molecules. The dashed lines represent probable hydrogen bonds. (**A**); CYP with ligand **18** (cyan). (**B**) and (**C**); two binding modes of CYP121 with ligand **17** (wheat).

The 2-methyl substituted analogue **17** exhibits two binding conformations (Figure 6B and C). The first binding conformation is similar to the binding mode for 2,6-dimethylated analogue **18**. The second binding mode for the 2-methylated analogue **17** is similar to that of the 3,5-dimethyl analogue **16** with the substituted aromatic ring in the pocket near the heme prosthetic group.

The 3-F analogue **14** binds in a similar manner to natural substrate **1**, with the substituted aromatic ring binding in the distal pocket (Figure 7). Two bound conformations are observed: one binding mode is similar to the 3-methyl substituted analogue **15** with the fluoro substituent facing toward the Thr77 residue. In the second binding mode, the substituted aromatic ring is flipped so that the fluoro substituent is facing towards the Gln385 residue. The second binding mode is only possible because the small size of the fluorine atom allows it to be accommodated within the active site in the rotated conformation. All hydrogen bonding interactions, through a network of water

molecules, are similar for both binding conformations of analogue **14**, and are the same as those observed for the 3-methyl analogue **15**.

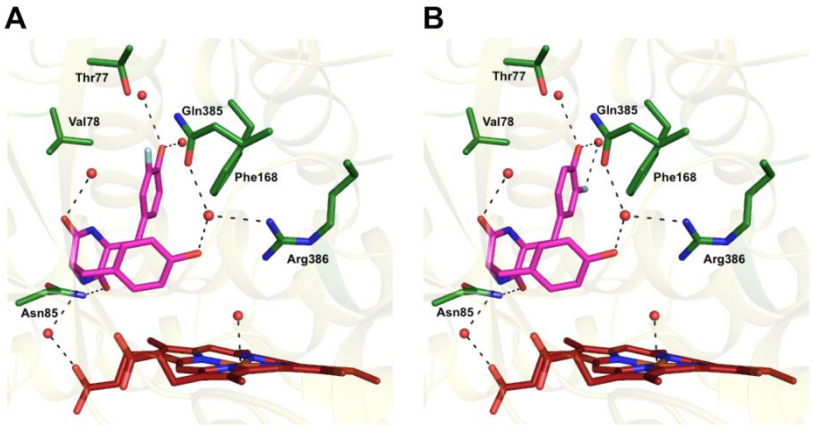

Figure 7: X-ray crystal structures of the 3-fluoro analogue **14** bound to CYP121 (PDB ID 6RQ6). The heme group is in red and the protein side chains are in green. The red spheres denote water molecules. The dashed lines represent probable hydrogen bonds. (**A**) and (**B**); two binding modes of CYP121 with ligand **14** (magenta).

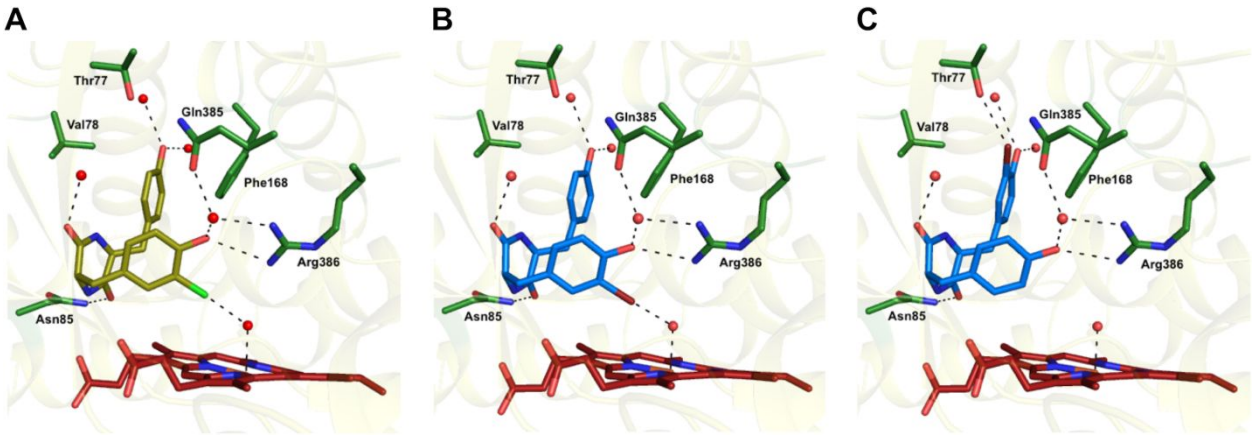

Figure 8: X-ray crystal structures of the 3-chloro analogue **13** and 3-bromo analogue **12** bound to CYP121 (PDB IDs 6RQD, 6RQB). The heme group is in red and the protein side chains are in green. The red spheres denote the water molecules. The dashed lines represent probable hydrogen

bonds. (**A**); CYP with ligand **13** (olive). (**B**) and (**C**); two binding modes of CYP121 with ligand **12** (blue).

The 3-Cl and 3-Br analogues, **13** and **12**, bind in a similar manner to natural substrate **1**, but in contrast to the fluoro analogue **14** the halogen-substituted aromatic ring binds in the heme pocket (Figure 8). The binding of the ligands does not displace the water molecule associated with the Fe^{III} ion as the sixth ligand, and potential interactions between the halogen and the water molecule are observed in each case. Two bound conformations are observed for the 3-bromo analogue **12**: one with the bromo substituent in the heme binding pocket and the other with the bromo substituent facing towards the Thr77 residue in the pocket distal to the heme.

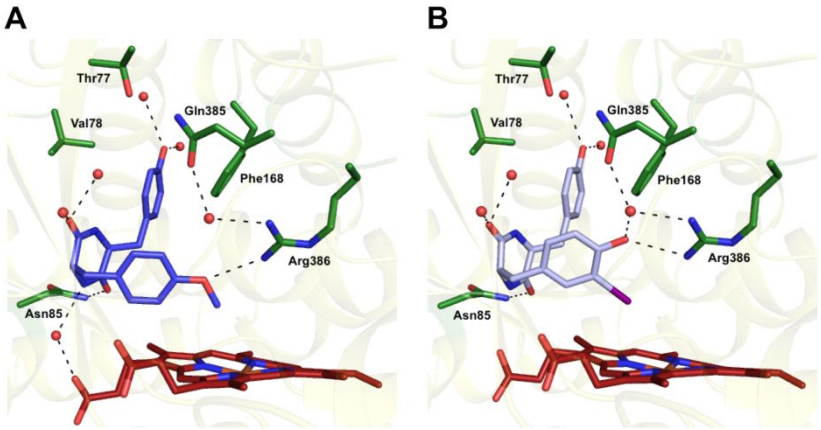

Figure 9: X-ray crystal structures of the 4-*O*-methyl analogue **5** and 3-iodo analogue **11** bound to CYP121 (PDB IDs 6RQ9, 6RQ8). The heme group is in red and the protein side chains are in green. The red spheres denote the water molecules. The dashed lines represent probable hydrogen bonds. (**A**); CYP with ligand **5** (blue). (**B**); CYP121 with ligand **11** (light blue).

For the 4-*O*-methyl analogue **5** the substituted aromatic ring binds in the proximal pocket close to the heme, with the *O*-methyl group situated very close to the heme Fe^{III} ion (Figure 9A). The sixth (distal) H_2O ligand is completely displaced, which correlates with the large high-spin signal observed in both the EPR and UV-visible spectra. The aromatic side chain rotates down slightly towards the heme Fe^{III} ion so that the OMe group is directly above the Fe ion. It may be speculated that there are specific CH_3–Fe interactions between the *O*-methyl hydrogens and the Fe^{III} ion that contribute to the high binding affinity.[37] The OMe moiety is also participating in a direct hydrogen-bonding interaction with Arg386, bringing the ligand closer to the heme group.

The 3-iodo analogue **11** also binds with the substituted aromatic ring in the proximal pocket, with the sixth H_2O ligand completely displaced (Figure 9B). The iodine atom is situated very close to the heme Fe^{III} ion occupying the space otherwise occupied by the H_2O ligand, which again correlates with the large high-spin signal observed in both the EPR and UV-visible spectra. The phenolic group on the substituted aromatic ring is within hydrogen-bonding distance of Arg386 which indicates tight binding and also correlates with the high binding affinity observed for this compound.

Turnover experiments

Turnover experiments were undertaken for compounds **2**–**18**, but they failed to show any significant level of CYP-catalyzed turnover for any compound except natural substrate cYY **2**.

Antimicrobial assays

Most of the synthesized substrate analogues have a greater binding affinity for CYP121 than the natural substrate cYY **1**, with the iodinated analogues **8**, **9** and **11** exhibiting up to a 100-fold

greater binding affinity. It was therefore envisaged that these analogues might be able to function as competitive inhibitors of CYP121 in vitro, thereby exerting anti-mycobacterial activity.

Various analogues were therefore tested for their MIC values in a resazurin-based Mtb cell viability assay. Mtb H37Rv at an OD of 0.001 and the bacterial suspension was incubated with the compounds at different dilutions for 7 days. Resazurin was then added to the wells and incubated for a further 24 hours, and then the Mtb survival was calculated as a percentage of negative controls.[38] Unfortunately, all compounds exhibited little or no antimicrobial activity with MIC values greater than 100 μM (see SI). The dense, waxy cell wall of Mtb presents a major obstacle to the penetration of molecules into the bacterial cell, which is a possible cause of the lack of activity of the assayed compounds. Further modifications are underway to develop compounds with better mycobacterial cell penetration.

DISCUSSION

The binding affinities of substrate analogues containing modifications at the phenolic group (4-position) of the aromatic rings were scrutinized for structure-activity relationships of these modifications. Firstly, it is apparent that the phenolic groups of substrate cYY **1** are not essential for binding. Compounds with one or both phenols either removed, methylated or replaced with iodine display similar or increased binding affinity. Removal of one phenol to give cYF results in a decreased binding affinity, as may be expected with the loss of binding interactions (van der Waals and hydrogen bonding) with this OH group. However, there is no apparent explanation for the increased binding affinity of cFF which lacks both phenolic groups: no increase in binding interactions are evident, and no high spin enzyme adduct is formed upon binding. Blocking of one phenol with a methyl ether (compound **5**) results in 3-fold improved binding and a large shift to

high spin Fe^{III} upon binding. X-ray crystallographic analysis shows that this is due to the OMe group occupying the space of the 6th ligand water molecule, with possible OMe–Fe interactions accounting for the improved binding. The bis-OMe compound **6** also induced a large shift to high spin Fe^{III}, though it has slightly weaker binding than **5**. Though X-ray data were not available for CYP121 bound to **6**, presumably the proximal pocket interacts with **6** in much the same way as **5** (with favourable interactions of the CH_3 group with the heme Fe^{III}), with the additional OMe group in the distal pocket resulting in the loss of a H-bond donor, thereby accounting for the slight loss of affinity.

The 4-F and 4-I compounds **7** and **8** both display increased binding affinity compared with cYY **1**. The fluoro analogue **7** displays an anomalous sigmoidal UV-Vis trace, which suggests allosteric binding interactions. However, as the EPR spectrum shows little shift to high spin state and no X-ray data could be obtained, little interpretation of this behavior can be postulated. The iodo analogue **8** results in a moderate amount of the high spin state upon binding, and high binding affinity. Though no X-ray data are available, the data for the 3-I compound **11** (vide infra) suggest that the 4-I compound **8** binds with the iodine atom close to the heme Fe^{III}, such that 'halogen binding' is invoked, and that this compound possibly displaces the 6th ligand water molecule.

The aryl-methylated compounds **15**–**18** provide us with information regarding the steric effects of substrate binding to CYP121. Substituents at the 2-position of the aromatic ring are not well tolerated. Though introduction of a single 2-Me substituent on the ring results in only a slight decrease in binding affinity, the X-ray data demonstrate that, when binding in the standard orientation and in order to avoid unfavorable interactions with the heme, the 2-Me group is forced to be positioned close to the DKP carbonyl oxygen. Hence, a flipped binding conformation, where the DKP ring and the tyrosyl side chain essentially swap positions, becomes a competitive binding

orientation. In the 2,6-diMe compound **18**, binding in the standard orientation becomes highly unfavorable, as one of the Me substituents would have a severe steric clash with the heme group. Accordingly, this compound binds only in the flipped conformation, though only very weakly (K_D > 100 μM).

The 3-Me substituted analogue **15** displays excellent affinity for CYP121, and induces a moderate amount of high spin Fe^{III} upon binding. In contrast the 3,5-dimethyl compound **16** exhibits moderate binding affinity, yet induces a high amount of the high spin state. The X-ray data enable an explanation to be forthcoming, which highlights the intriguing variations that can arise when a symmetrical substrate (or pseudo-symmetrical substrate analogue) binds to an asymmetric active site. The 3-Me analogue **15** binds with the Me-substituted aromatic ring in the distal binding pocket. The increase in binding affinity is presumably a result of increased hydrophobic binding interactions of the additional Me group with Phe168 and Val78. The standard tyrosyl group binds adjacent to the heme in the proximal pocket, such that only a moderate amount of high spin Fe^{III} is induced. In contrast the 3,5-diMe analogue **16** binds in two conformations, with the substituted aromatic ring equally disposed to binding in the distal pocket or the proximal pocket. Additional hydrophobic interactions may be gained upon binding in the distal pocket, while in the proximal pocket one of the Me groups binds close to the heme Fe. Though the X-ray structure shows the 6^{th} ligand water is still in place, steric interactions with the 3-Me substituent may favor its displacement, thereby increasing the conversion to the high-spin Fe state. The second methyl group (5-Me) in each conformation gives rise to slightly unfavorable interactions such that the overall binding affinity is weaker than the 3-Me analogue **15**.

The 3-halo analogues **9** and **11**–**14** all bind with increased affinity relative to **1**, with the smallest improvement being for the fluoro compound **14** and then a stepwise increase in affinity with

increasing size to the iodo compound **11** (i.e. K_D F<Cl<Br<I). The difference observed for the halogenated analogues may be due to steric and/or electronic effects. Analysis of the X-ray data for the 3-F analogue **14** shows the fluorinated aromatic ring binds in the pocket away from the heme group, and in both conformations – i.e. with the C–F bond pointing towards helix I or away from it. Presumably the small size of the fluorine atom results in insignificant steric clashes with nearby active site residues, with minor increases in van der Waals contacts resulting in slightly improved binding affinity, relative to **1**. No significant electronic influence is apparent, as the electron withdrawing fluorine group should have a greater impact on hydrogen bonding from the adjacent phenol than the other halogens. The 3-Cl and 3-Br analogues, **13** and **12**, bind with the halogen in the heme pocket: though they do not displace the heme Fe^{III} 6th ligand water molecule, the halogens interact with the water molecule in a manner similar to that reported for the nitrile moiety of bicalutamide to CYP46A1.[39] The 3-I analogue **11** binds with the substituted ring situated close to the heme prosthetic group. The iodine atom is situated very close to the heme Fe^{III} and intriguingly this analogue displaces the 6th ligand water molecule upon binding. This observation is in good correlation with both the UV-Vis and EPR spectroscopic data, which show the enzyme undergoes an almost complete shift to the high-spin state upon binding **11**. It is interesting to compare the 3-I, 3-Br and 3-Me analogues, which all exhibit tight binding to CYP121 (1.1, 0.5, 0.3 μM, respectively). The size of an iodine substituent is slightly larger than a Me group (2.15 vs 2.00 Å), with a bromine substituent (1.95 Å) slightly smaller than a methyl group. Could van der Waals interactions thus account for the difference in affinity? The X-ray data show that this is not the case, with **11**, **12** and **15** binding in different orientations. The smallest substituent, the 3-Br group of **12**, binds in two conformations; either away from the heme or in the pocket close to the heme but without displacing the water ligand. The slightly larger substituent, the 3-Me group of

15, only binds in the pocket away from the heme, whereas the largest group, the 3-I of **11**, binds in the pocket close to the heme and does displace the water ligand. Thus, we presume that the iodine, due to its large size and polarizability, binds such that favorable halogen-bonding interactions with the heme group give rise to sub μM level binding affinity.[40] The 3-Br and 3-Cl analogues **12** and **13**, bind in a similar fashion, with decreased size and polarizability (c.f. 3-I) resulting in gradually poorer affinity and a lack of displacement of the water molecule. The non-polarizable 3-F substituent binds with the substituted aromatic ring in the pocket distal to the heme, where small improvements in van der Waals contacts give a marginal improvement in binding affinity.

CONCLUSION

In conclusion, we have synthesized and analyzed a family of analogues of the substrate of the *Mtb* CYP121 enzyme to unveil structural information about this enzyme and its ligands. CYP121 in the presence of these analogues was analyzed by UV-Vis and EPR spectroscopy, and by X-ray crystallography, yielding information on the binding affinity of the substrate analogues, enzyme Fe^{III} spin state and the active site structure. The introduction of a single iodine atom onto the substrate of CYP121 results in sub-μM binding affinity and a complete shift to the high spin state of the heme Fe^{III}. We speculate that the high binding affinity of the 3-iodo analogue **11** is a result of a specific interaction between the iodine atom and either the Fe^{III} ion or the heme group, such as 'halogen bonding' or 'σ-hole bonding'.[40] The introduction of halogens that are able to interact with heme groups is thus a reasonable approach to the development of next-generation, tight binding inhibitors of the CYP121 enzyme, in the search for novel anti-tubercular compounds.

EXPERIMENTAL SECTION

General experimental methods

Commercially available reagents and solvents were used without further purification unless otherwise stated. Acetone was dried over calcium sulfate, potassium carbonate was dried in a hot air oven (130 °C) overnight. Molecular sieves were activated with a conventional microwave and allowed to cool under vacuum. DMF was dried over activated sieves (4 Å) for 16 h before use. Progress of the reactions was monitored by analytical thin-layer chromatography using Merck pre-coated silica gel 60 aluminium plates with F254 indicator. Visualization of spots was accomplished by using UV light (254 nm), DNPH (2,4-dinitrophenyl hydrazine), *p*-anisaldehyde or phosphomolybdic acid stain. Purification of crude mixtures was performed by flash chromatography on silica gel 40–63 μm with eluting solvents reported as % v/v mixtures. Yields refer to chromatographically and spectroscopically pure compounds, unless otherwise indicated. All compounds were determined to be of >95% purity by ^{1}H NMR analysis. ^{1}H NMR and ^{13}C NMR spectra were recorded in $CDCl_3$, CD_3OD or d_6-dimethyl sulfoxide (DMSO-d_6) solution, on a Varian Unity Inova 400 (400 MHz ^{1}H, 100 MHz ^{13}C) or 500 (500 MHz ^{1}H, 125 MHz ^{13}C) spectrometer. Chemical shift values (δ) are reported in ppm relative to $CHCl_3$ (δ = 7.26 ppm), DMSO-d_6 (δ = 2.50 ppm) and CD_3OD (δ = 3.31 ppm) for ^{1}H NMR and relative to the central $CDCl_3$ resonance (δ = 77.16 ppm), central DMSO-d_6 resonance (δ = 39.52 ppm) and central MeOD resonance (δ = 49.00 ppm) for ^{13}C NMR. The proton spectra are reported as follows δ (multiplicity, coupling constant *J* in Hz, number of nuclei). Multiplicities are indicated by s (singlet), d (doublet), dd (doublet of doublet), dt (doublet of triplet), dq (doublet of quartet), t (triplet), q (quartet), m (multiplet) and br s (broad singlet), etc. Mass spectra were recorded using a NanoLC/OrbiTrap Fusion™ Lumos™ spectrometer.

General procedure A: Synthesis of DKPs

The Boc dipeptide methyl ester was dissolved in formic acid (5 mL/mmol) and stirred at room temperature. When the Boc-deprotection was complete (by TLC analysis, 2–3 hours) formic acid was evaporated under reduced pressure. A mixture of *sec*-butanol and toluene (1:4, 0.01 M) was added and the solution was heated at 90 °C for 4 h. The solvent was evaporated under reduced pressure to yield an off-white solid. Trituration of the solid with ethyl acetate afforded the pure DKP.

General procedure B: Synthesis of *N*-acetyl-(α,β-dehydro)-DKPs

To a solution of *N*,*N*-diacetyl-cyclo(glycine-L-tyrosine(OBn)) (394 mg, 1 mmol) in dry DMF (3 mL) under nitrogen atmosphere was added Cs_2CO_3 (326 mg, 1 mmol), the benzaldehyde derivative (2 mmol) and molecular sieves 3Å (100 mg). The reaction mixture was stirred at room temperature until the reaction was complete. The reaction mixture was diluted with water (300 mL) and then extracted with ethyl acetate (3 × 100 mL). The aqueous layer was discarded and the ethyl acetate layer was washed with brine (3 × 50 mL), dried over $MgSO_4$, filtered and evaporated under reduced pressure to afford the crude product. The crude product was purified by flash chromatography, eluting with a gradient of 20–30% ethyl acetate in hexane to obtain the olefin.

General procedure C: Synthesis of *N*-acetyl DKPs

To a solution of olefin (1 equiv.) in ethyl acetate/methanol (1:1, 0.01 M) was added 10% Pd/C (50% by weight) and the reaction mixture was stirred at room temperature under a hydrogen atmosphere until the reaction was complete. The reaction mixture was filtered through a silica plug

followed by removal of the solvent under reduced pressure to obtain the crude product. The crude product was purified by flash chromatography using 5% MeOH in DCM to obtain the *N*-acetyl DKP.

General procedure D: *N*-Acetyl deprotection

The *N*-acetyl DKP (1 equiv.) was stirred in 10% aqueous NH_3 (0.2 M) for 15 minutes followed by removal of aqueous NH_3 by lyophilization. The crude product was purified by flash chromatography in 10–20% MeOH in DCM.

cyclo(L-Tyrosine-L-tyrosine) 1

The title compound was prepared from Boc-L-tyrosine-L-tyrosine-OMe (688 mg, 1.5 mmol) according to general procedure A and was obtained as a white solid (450.0 mg, 92%). M.p. 288–290 °C (lit. m.p. 270–275 °C).[24] ^{1}H-NMR (400 MHz, DMSO-d_6): δ 9.20 (s, 2H), 7.76 (d, J = 2.0 Hz, 2H), 6.84 (d, J = 8.4 Hz, 4H), 6.67 (d, J = 8.4 Hz, 4H), 3.85–3.83 (m, 2H), 2.53 (dd, J = 4.6 Hz, 2H, partially obscured by DMSO peak), 2.10 (dd, J = 13.7, 6.5 Hz, 2H). ^{13}C-NMR (125 MHz, DMSO-d_6): δ 166.2, 156.0, 130.7, 126.5, 115.0, 55.7, 38.8. NMR data consistent with that reported.[24] HRMS (ESI) calcd. for $C_{18}H_{19}N_2O_4^+$ [(M+H)$^+$] 327.1345, found 327.1346.

cyclo(L-Phenylalanine-L-tyrosine) 3

The title compound was prepared from Boc-L-phenylalanine-L-tyrosine-OMe (664 mg, 1.5 mmol) according to general procedure A and was obtained as a white solid (399.0 mg, 86%). M.p. 290–293 °C (lit. m.p. 291–293 °C).[41] ^{1}H-NMR (400 MHz, DMSO-d_6): δ 9.22 (s, 1H), 7.85 (br s, 2H), 7.29–7.18 (m, 3H), 7.03 (d, J = 7.1 Hz, 2H), 6.83 (d, J = 8.4 Hz, 2H), 6.67 (d, J = 8.3 Hz,

2H), 3.94 (m, 1H), 3.89 (m, 1H), 2.58 (dd, J = 13.6, 4.8 Hz, 1H), 2.22–2.15 (m, 2H), one dd obscured by the DMSO peak. ^{13}C-NMR (125 MHz, DMSO-d_6): δ 166.3, 166.2, 156.1, 136.6, 130.8, 129.7, 128.2, 126.5, 126.4, 115.0, 55.7, 55.4, 38.5, (one ^{13}C peak obscured by DMSO). NMR data consistent with that reported.[42] HRMS (ESI) calcd. for $C_{18}H_{19}N_2O_3^+$ [(M+H)$^+$] 311.1390, found 311.1390.

cyclo(L-Phenylalanine-L-phenylalanine) 4

The title compound was prepared from Boc-L-phenylalanine-L-phenylalanine-OMe (640 mg, 1.5 mmol) according to general procedure A and was obtained as a white solid (396 mg, 90%). M.p. 296–298 °C (lit. m.p. 297–300 °C).[43] ^{1}H-NMR (400 MHz, DMSO-d_6): δ 7.92 (br s, 2H), 7.30–7.19 (m, 6H), 7.04 (d, J = 7.1 Hz, 4H), 3.95–3.94 (m, 2H), 2.57 (dd, J = 13.6, 4.8 Hz, 2H), 2.23 (dd, J = 13.6, 6.2 Hz, 2H). ^{13}C-NMR (100 MHz, DMSO-d_6): δ 166.2, 136.6, 129.8, 128.2, 126.5, 55.4, 39.4. NMR data consistent with that reported.[44]

cyclo(L-Tyrosine(OMe)-L-tyrosine) 5

The title compound was prepared from the mixture of regoisomers **21b** (270 mg, 0.57 mmol) according to general procedure A and was obtained as a white solid (131.0 mg, 68%). M.p. 252–254 °C. ^{1}H-NMR (400 MHz, DMSO-d_6): δ 9.22 (s, 1H), 7.83 (br s, 1H), 7.80 (br s, 1H), 6.95 (d, J = 8.6 Hz, 2H), 6.86–6.83 (m, 4H), 6.68 (d, J = 8.5 Hz, 2H), 3.88 (m, 2H), 3.70 (s, 3H), 2.56–2.50 (m, 2H), 2.21–2.08 (m, 2H). ^{13}C-NMR (100 MHz, DMSO-d_6): δ 166.26, 166.24, 158.0, 156.1, 130.8, 130.8, 128.5, 126.5, 115.0, 113.7, 55.7, 55.6, 55.0, 39.5, 38.6. HRMS (ESI) calcd. for $C_{19}H_{21}N_2O_4^+$ [(M+H)$^+$] 341.1496, found 341.1496.

cyclo(L-Tyrosine(OMe)-L-tyrosine(OMe)) 6

The title compound was prepared from Boc-L-tyrosine(OMe)-L-tyrosine(OMe)-OMe **21c** (500 mg, 1.03 mmol) according to general procedure A and was obtained as a white solid (258.0 mg, 71%). M.p. 278–281 °C. ^{1}H-NMR (400 MHz, DMSO-d_6): δ 7.86 (br s, 2H), 6.94 (d, J = 8.5 Hz, 4H), 6.84 (d, J = 8.5 Hz, 4H), 3.91 (m, 2H), 3.69 (s, 6H), 2.55 (dd, J = 13.7, 4.6 Hz, 2H), 2.21 (dd, J = 13.7, 6.1 Hz, 2H). ^{13}C-NMR (100 MHz, DMSO-d_6): δ 166.2, 158.0, 130.8, 128.4, 113.7, 55.6, 55.0, 38.4. HRMS (ESI) calcd. for $C_{20}H_{21}N_2O_4^-$ [(M–H)$^-$] 353.1507, found 353.1494.

cyclo(4-Fluoro-L-phenylalanine-4-fluoro-L-phenylalanine) 7

The title compound was prepared from Boc-4-fluoro-L-phenylalanine-4-fluoro-L-phenylalanine-OMe (694 mg, 1.5 mmol) according to general procedure A and was obtained as a white solid (439 mg, 89%). M.p. 282–284 °C. ^{1}H-NMR (400 MHz, DMSO-d_6): δ 8.03 (s, 2H), 7.09–7.01 (m, 8H), 4.01 (m, 2H), 2.60 (dd, J = 13.7, 4.8 Hz, 2H), 2.41 (dd, J = 13.7, 5.6 Hz, 2H). ^{13}C-NMR (100 MHz, DMSO-d_6): δ 166.6, 161.6 (d, J = 242.14 Hz), 132.9 (d, J = 2.95 Hz), 132.0 (d, J = 8.11 Hz), 115.3 (d, J = 21.12 Hz), 55.7, 38.4. HRMS (ESI) calcd. for $C_{18}H_{17}F_2N_2O_2^+$ [(M+H)$^+$] 331.1253, found 331.1253.

cyclo(4-Iodo-L-phenylalanine-4-iodo-L-phenylalanine) 8

The title compound was prepared from Boc-4-iodo-L-phenylalanine-4-iodo-L-phenylalanine-OMe (1.02 g, 1.5 mmol) according to general procedure A and was obtained as a white solid (717 mg, 88%). M.p. 285–288 °C. ^{1}H-NMR (400 MHz, DMSO-d_6): δ 8.03 (s, 2H), 7.63 (d, J = 8.0 Hz, 4H), 6.84 (d, J = 8.0 Hz, 4H), 4.02 (br s, 2H), 2.57 (dd, J = 13.7, 4.8 Hz, 2H), 2.36 (dd, J = 13.7, 5.7 Hz, 2H). ^{13}C-NMR (125 MHz, DMSO-d_6): δ 166.1, 136.9, 136.3, 132.1, 92.5, 54.9, 38.4.

cyclo(3-Iodo-L-tyrosine-3-iodo-L-tyrosine) 9

The title compound was prepared from Boc-3-iodo-L-tyrosine-3-iodo-L-tyrosine-OMe (532.7 mg, 0.75 mmol) according to general procedure A and was obtained as an off-white solid (358.0 mg, 83%). ^{1}H-NMR (500 MHz, DMSO-d_6): δ 10.13 (br s, 1 H), 7.94 (d, *J* = 2.4 Hz, 1 H,), 7.36 (d, *J* = 2.2 Hz, 1 H,), 6.86 (dd, *J* = 8.4, 2.2 Hz, 1 H), 6.79 (d, *J* = 8.4 Hz, 1 H), 3.87 (m, 1H), 2.49 (dd, *J* = 14.0, 5.0 Hz, 1 H), 2.14 (dd, *J* = 14.0, 6.2 Hz, 1 H). ^{13}C-NMR (125 MHz, DMSO-d_6) δ 166.1, 155.4, 139.6, 131.0, 129.0, 114.6, 84.4, 55.6, 38.3.[24] HRMS (ESI) calcd. for $C_{18}H_{15}I_2N_2O_4^-$ [(M–H)$^-$] 576.9127, found 576.9124.

cyclo(3,5-Diiodo-L-tyrosine-L-tyrosine) 10

The title compound was prepared from Boc-L-tyrosine-3,5-diiodo-L-tyrosine-OMe (532.7 mg, 0.75 mmol) according to general procedure A and was obtained as a white solid (372.0 mg, 86%). ^{1}H-NMR (400 MHz, DMSO-d_6): 9.24 (br s, 2H), 7.98 (s, 1H), 7.88 (s, 1H), 7.40 (s, 2H), 6.85 (d, *J* = 8.3 Hz, 2H), 6.67 (d, *J* = 8.3 Hz, 2H), 3.88 (m, 2H), 2.58 (dd, *J* = 13.7, 4.5 Hz, 1H), 2.41 (dd, *J* = 13.7, 4.8 Hz, 1H), 2.19 (dd, *J* = 13.6, 6.3 Hz, 1H), 2.09 (dd, *J* = 13.6, 7.2 Hz, 1H). ^{13}C-NMR (125 MHz, DMSO-d_6): δ 166.3, 165.9, 156.1, 154.1, 140.2, 132.6, 130.9, 126.4, 115.0, 86.8, 55.7, 55.3, 37.5 (one ^{13}C peak obscured by DMSO). HRMS (ESI) calcd. for $C_{18}H_{15}I_2N_2O_4^-$ [(M–H)$^-$] 576.9127, found 576.9125.

cyclo(L-Tyrosine-3-iodo-L-tyrosine) 11

The title compound was prepared from Boc-L-tyrosine-3-iodo-L-tyrosine-OMe (438.3 mg, 0.75 mmol) according to general procedure A and was obtained as a white solid (266.0 mg, 79%). ^{1}H-

NMR (500 MHz, DMSO-d_6): δ10.11 (br s, 1H), 9.21 (br s, 1H), 7.89 (br s, 1H), 7.81 (br s, 1H), 7.34 (d, *J* = 1.6 Hz, 1H), 6.86 (dd, *J* = 8.3, 1.6 Hz, 1H), 6.83 (d, *J* = 8.3 Hz, 2H), 6.79 (d, *J* = 8.2 Hz, 1H), 6.67 (d, *J* = 8.3 Hz, 2H), 3.86 (m, 2H), 2.54 (dd, *J* = 13.6, 4.4 Hz, 1H), 2.46 (dd, *J* = 13.7, 4.6 Hz, 1H), 2.14–2.08 (m, 2H). ^{13}C-NMR (125 MHz, DMSO-d_6): δ 166.3, 166.1, 156.1, 155.4, 139.8, 130.93, 130.84, 129.1, 126.4, 115.0, 114.7, 84.5, 55.73, 55.60, 38.2 (one ^{13}C peak obscured by DMSO). NMR data consistent with that reported.[45] HRMS (ESI) calcd. for $C_{18}H_{18}IN_2O_4^+$ [$(M+H)^+$] 453.0305, found 453.0305.

cyclo(L-Tyrosine-3-bromo-L-tyrosine) 12

The title compound was prepared from Boc-L-tyrosine-3-bromo-L-tyrosine-OMe (403.1 mg, 0.75 mmol) according to general procedure A and was obtained as a white solid (236 mg, 78%). M.p. 296–298 °C (lit. m.p. 297–300 °C).[45] ^{1}H-NMR (500 MHz, $CDCl_3$): δ 10.12 (br s, 1H), 9.53 (br s, 1H), 7.89 (d, *J* = 2.4 Hz, 1H), 7.84 (d, *J* = 2.4 Hz, 1H), 7.11 (d, *J* = 1.7 Hz, 1H), 6.87–6.82 (m, 4H), 6.66 (d, *J* = 8.5 Hz, 2H), 3.88–3.83 (m, 2H), 2.54 (dd, *J* = 13.7, 4.6 Hz, 1H), 2.46 (dd, *J* = 13.7, 4.7, 1H), 2.18 (dd, *J* = 13.7, 6.3 Hz, 1H), 2.05 (dd, *J* = 13.7, 6.5 Hz, 1H). ^{13}C-NMR (125 MHz, $CDCl_3$): δ 166.8, 166.6, 156.6, 153.3, 134.3, 131.3, 130.5, 129.1, 126.9, 116.6, 115.5, 109.5, 56.2, 55.4, 39.4, 38.9. NMR data consistent with that reported.[45] HRMS (ESI) calcd. for $C_{18}H_{18}BrN_2O_4^+$ [$(M+H)^+$] 405.0444, 407.0424 found 405.0444, 407.0423.

cyclo(L-Tyrosine-3-chloro-L-tyrosine) 13

The title compound was prepared from Boc-L-tyrosine-3-chloro-L-tyrosine-OMe (369.7 mg, 0.75 mmol) according to general procedure A and was obtained as a white solid (208 mg, 77%). ^{1}H-NMR (500 MHz, DMSO-d_6): δ 7.87 (br d, *J* = 2.6 Hz, 1H), 7.86 (br d, *J* = 2.5 Hz, 1H), 6.96

(d, *J* = 2.1 Hz, 1H), 6.87 (d, *J* = 8.2 Hz, 1H), 6.84 (d, *J* = 8.5 Hz, 2H), 6.78 (dd, *J* = 8.3, 2.1 Hz, 1H), 6.67 (d, *J* = 8.5 Hz, 2H), 3.90–3.84 (m, 2H), 2.56 (dd, *J* = 13.7, 4.6 Hz, 1H), 2.46 (dd, *J* = 13.7, 4.8 Hz, 1H), 2.22 (dd, *J* = 13.7, 6.2 Hz, 1H), 2.03 (dd, *J* = 13.7, 6.7 Hz, 1H). ^{13}C-NMR (125 MHz, DMSO-d_6): δ 166.3, 166.1, 156.1, 151.9, 130.9, 130.8, 129.3, 128.1, 126.4, 119.2, 116.4, 115.0, 55.7, 55.5, 38.8, 38.5. HRMS (ESI) calcd. for $C_{18}H_{18}ClN_2O_4^+$ [$(M+H)^+$] 361.0950, found 361.0950.

cyclo(L-Tyrosine-3-fluoro-L-tyrosine) 14

The title compound was prepared from the corresponding *N*-acetyl DKP (77 mg, 0.2 mmol) using general procedure D and was obtained as a white solid (52 mg, 76%). ^{1}H-NMR (500 MHz, DMSO-d_6): δ 9.62 (s, 1H), 9.22 (s, 1H), 7.87 (br d, *J* = 2.1 Hz, 1H), 7.81 (br d, *J* = 2.1 Hz, 1H), 6.87–6.82 (m, 3H), 6.75 (dd, *J* = 12.3, 2.0 Hz, 1H), 6.68 (d, *J* = 6.8 Hz, 2H), 6.62 (dd, *J* = 8.2, 2.0 Hz, 1H), 3.90 (m, 1H), 3.84 (m, 1H), 2.57 (dd, *J* = 13.7, 4.7 Hz, 1H), 2.47 (dd, *J* = 13.6, 4.7 Hz, 1H), 2.29 (dd, *J* = 13.7, 5.9 Hz, 1H), 1.94 (dd, *J* = 13.7, 7.0 Hz, 1H). ^{13}C-NMR (125 MHz, DMSO-d_6): δ 166.7, 166.6, 156.6, 151.1 (d, J = 238.9 Hz), 143.9 (d, 12.1 Hz), 131.3, 128.3 (d, 5.9 Hz), 126.8, 126.2 (d, 3.0 Hz), 117.9 (d, 3.1 Hz), 117.6 (d, 17.8 Hz), 115.5, 56.1, 56.0, 39.1 (1 obscured). HRMS (ESI) calcd. for $C_{18}H_{16}FN_2O_4^-$ [$(M–H)^-$] 343.1100, found 343.1101.

cyclo(L-Tyrosine-3-methyl-L-tyrosine) 15

The title compound was prepared from the corresponding *N*-acetyl DKP (77 mg, 0.2 mmol) using general procedure D and was obtained as an off-white solid (54 mg, 80%). M.P. 240–242 °C. ^{1}H-NMR (500 MHz, DMSO-d_6): δ 9.20 (s, 1H), 9.08 (s, 1H), 7.74 (m, 2H), 6.81 (d, *J* = 8.5 Hz, 2H), 6.74 (s, 1H), 6.68–6.66 (m, 4H), 3.86–3.82 (m, 2H), 2.52–2.50 (m, 2H, partly obscured

by DMSO peak), 2.11–2.08 (m, 1H, partly obscured), 2.08 (s, 3H), 2.06 (dd, J = 11.9, 4.9 Hz, 1H). ^{13}C-NMR (125 MHz, DMSO-d_6): δ 166.28, 166.26, 156.1, 154.1, 132.1, 130.7, 128.0, 126.5, 126.4, 123.4, 115.0, 114.3, 55.79, 55.73, 38.9, 16.1 (one ^{13}C peak obscured by the DMSO peak). HRMS (ESI) calcd. for $C_{19}H_{19}N_2O_4^-$ [(M–H)$^-$] 339.1350, found 339.1352.

cyclo(L-Tyrosine-3,5-dimethyl-L-tyrosine) 16

The title compound was prepared from the corresponding *N*-acetyl DKP (79.3 mg, 0.2 mmol) using general procedure D and was obtained as an off-white solid (58 mg, 82%). M.P. 220–224 °C. ^{1}H-NMR (500 MHz, DMSO-d_6): δ 9.20 (s, 1H), 8.03 (s, 1H), 7.74 (m, 2H), 6.79 (d, J = 8.5 Hz, 2H), 6.67 (d, J = 8.6 Hz, 2H), 6.59 (s, 2H), 3.86–3.81 (m, 2H), 2.47–2.50 (m, 2H), 2.12 (s, 6H), 2.01–2.08 (m, 2H). ^{13}C-NMR (125 MHz, DMSO-d_6): δ 166.27, 166.24, 156.0, 151.9, 130.7, 129.7, 126.6, 126.5, 123.8, 115.0, 55.7 (2C), 38.92, 38.87, 16.7. HRMS (ESI) calcd. for $C_{20}H_{21}N_2O_4^-$ [(M–H)$^-$] 353.1507, found 353.1506.

cyclo(L-Tyrosine-2-methyl-L-tyrosine) 17

The title compound was prepared from the corresponding *N*-acetyl DKP (77 mg, 0.2 mmol) using general procedure D and was obtained as a white solid (55 mg, 81%). M.P. 277–279 °C. ^{1}H-NMR (500 MHz, DMSO-d_6): δ 9.20 (s, 1H), 9.07 (s, 1H), 7.91 (d, J = 2.5 Hz, 1H), 7.68 (d, J = 2.6 Hz, 1H), 6.89 (d, J = 8.3 Hz, 2H), 6.69–6.67 (m, 3H), 6.51 (d, J = 2.4 Hz, 1H), 6.49 (dd, J = 8.2, 2.5 Hz, 1H), 3.91 (m, 1H), 3.74 (m, 1H), 2.59 (dd, J = 12.9, 4.0 Hz, 1H), 2.55–2.50 (m, 1H), 2.34 (dd, J = 13.7, 6.0 Hz, 1H), 2.09 (s, 3 H), 1.97 (dd, J =14.0, 7.2 Hz, 1H). ^{13}C-NMR (125 MHz, DMSO-d_6): δ 166.5, 166.1, 156.1, 155.9, 137.6, 131.7, 130.9, 126.5, 125.2, 116.8, 115.0, 112.5,

55.9, 55.1, 38.6, 36.9, 19.3. HRMS (ESI) calcd. for $C_{19}H_{19}N_2O_4^-$ [(M–H)$^-$] 339.1350, found 339.1350.

cyclo(L-Tyrosine-2,6-dimethyl-L-tyrosine) 18

To a solution of cyclo(*N*-acetyl-L-tyrosine(OBn)-(α,β-dehydro)-2,6-dimethyl-L-tyrosine(OBn)) **25d** (159 mg, 0.4 mmol) in ethyl acetate/methanol (1:1, 50 mL) was added 10% Pd/C (80 mg) and the mixture was stirred under H_2 atmosphere (30 bar) until the reaction was complete. The reaction mixture was filtered through a silica plug followed by removal of the solvent under reduced pressure to obtain the crude product. The title compound was obtained as a white solid after purification by flash chromatography eluting with 20–30% MeOH in DCM (92 mg, 64%). M.P. 294–296 °C. ^{1}H-NMR (500 MHz, DMSO-d_6): δ 9.20 (s, 1H), 8.92 (s, 1H), 8.11 (br d, J = 2.7 Hz, 1H), 7.73 (br d, J = 3.1 Hz, 1H), 6.98 (d, J = 8.5 Hz, 2H), 6.68 (d, J = 8.6 Hz, 2H), 6.35 (s, 2H), 4.02 (m, 1H), 3.60 (m, 1H), 2.85 (dd, J = 13.8, 5.3 Hz, 1H), 2.78 (dd, J = 13.8, 4.7 Hz, 1H), 2.59 (dd, J = 14.3, 4.6 Hz, 1H), 2.03 (s, 6H), (one doublet of doublet obscured by the DMSO peak). ^{13}C-NMR (125 MHz, DMSO-d_6): δ 166.9, 166.1, 156.1, 155.2, 138.0, 131.0, 126.4, 124.6, 115.1, 114.8, 56.0, 55.2, 38.4, 34.9, 20.4. HRMS (ESI) calcd. for $C_{20}H_{21}N_2O_4^-$ [(M–H)$^-$] 353.1507, found 353.1505.

cyclo(L-tyrosine(OBn)-glycine) 22

The title compound was prepared from Boc-L-tyrosine(OBn)-glycine-OMe (4.4 g, 9.9 mmol) according to general procedure A and was obtained as a white solid (2.3 g, 75%). M.p 266–268 °C. ^{1}H-NMR (400 MHz, DMSO-d_6): δ 8.11 (br s, 1H), 7.87 (br s, 1H), 7.43–7.28 (m, 5H), 7.07 (d, J = 8.5 Hz, 2H), 6.93 (d, J = 8.5 Hz, 2H), 5.07 (s, 2H), 4.01 (m, 1H), 3.34 (dd, J = 13.6, 2.6

Hz, 2H), 3.03 (dd, *J* = 13.6, 4.3 Hz, 1H), 2.80 (app. d, *J* = 16.8 Hz, 2H). ^{13}C-NMR (100 MHz, DMSO-d_6): δ 167.2, 165.6, 157.3, 137.1, 131.1, 128.4, 127.98, 127.78, 127.69, 114.5, 69.2, 55.6, 43.7, 37.9. HRMS (ESI) calcd. for $C_{18}H_{19}N_2O_3^+$ [$(M+H)^+$] 311.1390, found 311.1395.

cyclo(*N*,*N*-Diacetyl-L-tyrosine(OBn)-glycine) 23

A suspension of **22** (2.33g, 7.5 mmol) in acetic anhydride (80 mL) was heated at 70 °C overnight followed by removal of acetic anhydride by evaporation under reduced pressure. The crude product was purified by recrystallization from MeOH to obtain the title compound as a white solid (2.1 g, 71%). M.p. 126–128 °C. ^{1}H-NMR (400 MHz, $CDCl_3$): δ 7.42–7.33 (m, 5H), 6.96 (d, *J* = 8.6 Hz, 2H), 6.89 (d, *J* = 8.6 Hz, 2H), 5.40 (m, 1H), 5.04 (s, 2H), 4.52 (d, *J* = 19.0 Hz, 1H), 3.30 (dd, *J* = 14.2, 4.3 Hz, 1H), 3.15 (dd, *J* = 14.2, 5.4 Hz, 1H), 2.58 (s, 3H), 2.56 (s, 3H), 2.54 (d, *J* = 19 Hz, 1H). ^{13}C-NMR (100 MHz, $CDCl_3$): δ 171.4, 171.3, 168.4, 166.3, 158.8, 136.6, 131.0, 128.7, 128.2, 127.6, 126.6, 115.7, 70.2, 59.5, 46.4, 38.2, 27.4, 27.1. HRMS (ESI) calcd. for $C_{22}H_{23}N_2O_5^+$ [$(M+H)^+$] 395.1602, found 395.1605. $[\alpha]_D$ –10.1 (c = 0.75, $CHCl_3$, T = 24.8 °C).

cyclo(*N*-Acetyl-L-tyrosine(OBn)-(α,β-dehydro)-3-methyltyrosine(OBn)) 25a

The title compound was prepared from **23** and 4-benzyloxy-3-methylbenzaldehyde **24a** (453 mg, 2 mmol) using general procedure B and obtained as a clear oil (420 mg, 75%). ^{1}H-NMR (400 MHz, $CDCl_3$): δ 7.56–7.24 (m, 10H), 7.02–6.98 (m, 4H), 6.86 (d, *J* = 8.1 Hz, 1H), 6.78 (d, *J* = 8.4 Hz, 2H), 6.56 (s, 1H), 5.35 (m, 1H), 5.1 (s, 2H), 4.84, 4.77 (ABq, *J* = 11.7 Hz, 2H), 3.25 (dd, *J* = 14.1, 3.8 Hz, 1H), 3.17 (dd, *J* = 14.1, 5.1 Hz, 1H), 2.61 (s, 3H), 2.27 (s, 3H). ^{13}C-NMR (100 MHz, $CDCl_3$): δ 172.5, 165.8, 161.1, 158.8, 157.7, 136.9, 136.8, 131.7, 131.3, 128.8, 128.6, 128.4, 128.2, 128.1, 127.6, 127.4, 127.2, 126.5, 124.8, 123.9, 119.5, 115.4, 111.9, 70.1 (2C), 58.3, 38.4,

27.3,16.7. HRMS (ESI) calcd. for $C_{35}H_{33}N_2O_5^+$ [$(M+H)^+$] 561.2384, found 561.2392. $[\alpha]_D$: –136.7 (c = 1, $CDCl_3$, T = 23.8 °C).

cyclo(*N*-Acetyl-L-tyrosine(OBn)-(α,β-dehydro)-3,5-dimethyltyrosine(OBn)) 25b

The title compound was prepared from **23** and 4-benzyloxy-3,5-dimethylbenzaldehyde **24b** (481 mg, 2 mmol) using general procedure B and was obtained as a white foam (437 mg, 76%). ^{1}H-NMR (400 MHz, $CDCl_3$): δ 7.56 (br s, 1H), 7.47–7.27 (m, 10H), 7.01 (d, *J* = 8.5 Hz, 2H), 6.82–6.79 (m, 4H), 6.55 (s, 1H), 5.36 (m, 1H), 4.89, 4.83 (ABq, *J* = 11.7 Hz, 2H), 4.80 (s, 2H), 3.28–3.15 (m, 2H), 2.62 (s, 3H), 2.28 (s, 6H). ^{13}C-NMR (100 MHz, $CDCl_3$): δ 172.3, 165.6, 160.7, 158.6, 156.5, 137.1, 136.7, 132.3, 131.6, 129.1, 128.59, 128.50, 128.20, 128.12, 127.93, 127.80, 127.2, 126.3, 124.5, 119.0, 115.2, 74.2, 69.9, 58.1, 38.2, 27.1, 16.6. HRMS (ESI) calcd. for $C_{36}H_{35}N_2O_5^+$ [$(M+H)^+$] 575.2541, found 575.2549. $[\alpha]_D$: –107.8 (c = 1, $CHCl_3$, T = 25.1 °C).

cyclo(*N*-Acetyl-L-tyrosine(OBn)-(α,β-dehydro)-2-methyltyrosine(OBn)) 25c

The title compound was prepared from **23** and 4-benzyloxy-2-methylbenzaldehyde **24c** (453 mg, 2 mmol) using general procedure B and was obtained as a clear oil (415 mg, 74%). ^{1}H-NMR (500 MHz, $CDCl_3$): δ 7.42–7.22 (m, 10H), 6.97 (d, *J* = 8.4 Hz, 2H), 6.87 (d, *J* = 8.5 Hz, 1H), 6.81–6.79 (m, 3H), 6.76 (dd, *J* = 8.5, 2.5 Hz, 1H), 6.64 (s, 1H), 5.30 (m, 1H), 5.03 (s, 2H), 4.88, 4.85 (ABq, *J* = 11.7 Hz, 2H), 3.22 (dd, *J* = 14.2, 3.8 Hz, 1H), 3.15 (dd, *J* = 14.2, 5.1 Hz, 1H), 2.59 (s, 3H), 2.11 (s, 3H). ^{13}C-NMR (125 MHz, $CDCl_3$): δ 172.5, 165.5, 160.6, 159.4, 158.7, 139.9, 136.8, 136.7, 131.7, 128.8 (2C), 128.6, 128.3, 128.1, 127.54, 127.46, 126.5, 124.9, 124.0, 117.9, 117.8, 115.3, 112.6, 70.14, 70.06, 58.3, 38.4, 27.3, 20.3. HRMS (ESI) calcd. for $C_{35}H_{33}N_2O_5^+$ [$(M+H)^+$] 561.2384, found 561.2392. $[\alpha]_D$ –139.1 (c = 1, $CHCl_3$, T = 24.8 °C).

cyclo(*N*-Acetyl-L-tyrosine(OBn)-(α,β-dehydro)-2,6-dimethyltyrosine(OBn)) 25d

The title compound was prepared from **23** and 4-benzyloxy-2,6-dimethylbenzaldehyde **24d** (481 mg, 2 mmol) using general procedure B and obtained as a white solid (406 mg, 71%). M.p. 144–146 °C. ^{1}H-NMR (400 MHz, $CDCl_3$): δ 7.43–7.32 (m, 10H), 6.98 (d, *J* = 8.6 Hz, 2H), 6.91 (br s, 1H), 6.86 (d, *J* = 8.6 Hz, 2H), 6.79 (s, 1H), 6.67 (s, 2H), 5.32 (m, 1H), 5.04 (s, 2H), 5.00 (s, 2H), 3.21–3.20 (m, 2H), 2.65 (s, 3H), 1.95 (s, 6H). ^{13}C-NMR (100 MHz, $CDCl_3$): δ 172.2, 165.0, 159.7, 159.0, 158.4, 137.9, 136.9, 131.4 (2C), 128.72, 128.68, 128.1, 127.6, 127.5, 126.8, 126.5, 122.8, 118.9 (2C), 115.2, 114.5, 70.0 (2C), 58.4, 38.3, 27.4, 20.4. HRMS (ESI) calcd. for $C_{36}H_{35}N_2O_5^+$ [$(M+H)^+$] 575.2541, found 575.2552. $[\alpha]_D$: –41.0 (c = 0.8, $CHCl_3$, T = 23.8 °C).

cyclo(*N*-Acetyl-L-tyrosine(OBn)-(α,β-dehydro)-3-fluorotyrosine(OBn)) 25e

The title compound was prepared from **23** and 4-benzyloxy-3-fluorobenzaldehyde **24e** (460.4 mg, 2 mmol) using general procedure B and obtained as a yellow oil (450 mg, 80%). ^{1}H-NMR (400 MHz, $CDCl_3$): δ 7.45–7.27 (m, 10H), 7.00–6.78 (m, 7H), 6.46 (s, 1H), 5.35 (m, 1H), 5.16 (s, 2H), 4.87, 4.81 (ABq, *J* = 11.7 Hz, 2H), 3.25 (dd, *J* = 14.2, 3.7 Hz, 1H), 3.17 (dd, *J* = 14.2, 5.0 Hz, 1H), 2.62 (s, 3H). ^{13}C-NMR (100 MHz, $CDCl_3$): δ 172.4, 165.8, 160.7, 158.8, 152.9 (*J* = 249.0 Hz), 147.5 (*J* = 10.6 Hz), 136.8, 136.0, 131.7, 128.9, 128.65, 128.52, 128.1, 127.51, 127.41, 126.3, 125.8 (*J* = 6.8 Hz), 125.0 (*J* = 3.4 Hz), 124.95, 117.5, 116.6 (*J* = 19.2 Hz), 115.90 (*J* = 2.2 Hz), 115.3, 71.4, 70.1, 58.3, 38.3, 27.3. HRMS (ESI) calcd. for $C_{34}H_{30}FN_2O_5^+$ [$(M+H)^+$] 565.2133, found 565.2143. $[\alpha]_D$: –189.5 (c = 1, $CHCl_3$, T = 22.3 °C).

cyclo(*N*-Acetyl-L-tyrosine-3-methyl-L-tyrosine)

The title compound was prepared from olefin **25a** (224 mg, 0.4 mmol) according to general procedure C with 5 bar of hydrogen atmosphere for 16 hours and was obtained as a clear oil (140 mg, 92%). ^{1}H-NMR (500 MHz, CD_3OD): δ 6.89 (d, *J* = 8.5 Hz, 2H), 6.82 (s, 1H), 6.76–6.74 (m, 3H), 6.69 (d, *J* = 8.1 Hz, 1H), 4.95 (m, 1H), 4.21 (dd, *J* = 8.7, 4.1 Hz, 1H), 2.73–2.65 (m, 3H), 2.50 (s, 3H), 2.17 (s, 3H), 1.75 (dd, *J* = 13.9, 8.7 Hz, 1H). ^{13}C-NMR (125 MHz, CD_3OD): δ 173.4, 170.6, 169.0, 157.9, 155.8, 133.2, 132.6, 129.0, 127.95, 128.77, 126.0, 116.5, 115.8, 59.6, 59.1, 40.2, 39.0, 27.3, 16.3. HRMS (ESI) calcd. for $C_{21}H_{23}N_2O_5^+$ [(M+H)$^+$] 383.1602, found 383.1604. $[\alpha]_D$: –17.2 (c = 2, MeOH, T = 25.8 °C).

cyclo(*N*-Acetyl-L-tyrosine-3,5-dimethyl-L-tyrosine)

The title compound was prepared from olefin **25b** (230 mg, 0.4 mmol) according to general procedure C with 5 bar of hydrogen atmosphere for 24 hours and was obtained as a clear oil (142 mg, 90%). ^{1}H-NMR (400 MHz, $CDCl_3$): δ 6.99 (d, *J* = 8.4 Hz, 2H), 6.82 (d, *J* = 8.4 Hz, 2H), 6.57 (s, 2H), 5.67 (s, 1H), 5.46 (s, 1H), 5.13 (t, *J* = 4.4 Hz, 1H), 4.79 (s, 1H), 3.98 (m, 1H), 3.24 (dd, *J* = 14.3, 3.7 Hz, 1H), 3.11 (dd, *J* = 14.2, 5.0 Hz, 1H), 2.84 (dd, *J* = 13.6, 3.0 Hz, 1H), 2.62 (s, 3H), 2.18 (s, 6H), 0.98 (dd, *J* = 13.5, 11.5 Hz, 1H). ^{13}C-NMR (100 MHz, $CDCl_3$): δ 171.1, 167.8, 165.5, 154.6, 150.7, 131.3, 128.3, 126.1, 125.8, 123.0, 115.0, 57.4, 57.1, 38.1, 36.7, 26.5, 15.1. HRMS (ESI) calcd. for [(M+H)$^+$] 397.1758, found 397.1762. $[\alpha]_D$: –10.1 (c = 0.75, MeOH, T = 25.8 °C).

cyclo(*N*-Acetyl-L-tyrosine-2-methyl-L-tyrosine)

The title compound was prepared from olefin **25c** (224 mg, 0.4 mmol) according to general procedure C with 5 bar of hydrogen atmosphere for 24 hours and was obtained as a clear oil (126 mg, 83%). ^{1}H-NMR (500 MHz, CD_3OD): δ 6.94 (d, *J* = 8.3 Hz, 2H), 6.78–6.76 (m, 3H), 6.60 (s,

1H), 6.57 (dd, *J* = 8.2, 2.1 Hz, 1H), 5.00 (t, *J* = 4.8 Hz, 1H), 4.13 (dd, *J* = 9.4, 3.4 Hz, 1H), 2.93 (d, *J* = 4.8 Hz, 2H), 2.82 (dd, *J* = 14.1, 3.5 Hz, 1H), 2.54 (s, 3H), 2.20 (s, 3H), 1.62 (dd, *J* = 14.0, 9.5 Hz, 1H). ^{13}C-NMR (125 MHz, CD_3OD): δ 173.6, 170.6, 168.9, 158.1, 157.6, 139.2, 132.91, 132.73, 127.6, 126.6, 118.4, 116.7, 114.0, 59.2, 58.6, 38.7, 38.2, 27.4, 19.8. HRMS (ESI) calcd. for $C_{21}H_{23}N_2O_5^+$ [(M+H)$^+$] 383.1602, found 383.1605. $[\alpha]_D$: –16.1 (c = 0.5, MeOH, T = 25.7 °C).

cyclo(*N*-Acetyl-L-tyrosine-3-fluoro-L-tyrosine)

The title compound was prepared from olefin **25e** (226 mg, 0.4 mmol) according to general procedure C with 4–5 bar of hydrogen atmosphere for 6 hours and was obtained as a clear oil (142 mg, 93%). ^{1}H-NMR (500 MHz, CD_3OD): δ 6.92 (d, *J* = 8.5 Hz, 2H), 6.85 (m, 1H), 6.80–6.76 (m, 3H), 6.70 (dd, *J* = 8.2, 1.6 Hz, 1H), 4.98 (m, 1H), 4.19 (dd, *J* = 9.1, 4.3 Hz, 1H), 2.86 (d, *J* = 3.9 Hz, 2H), 2.62 (dd, *J* = 13.9, 4.2 Hz, 1H), 2.52 (s, 3H), 1.54 (dd, *J* = 13.9, 9.1 Hz, 1H). ^{13}C-NMR (125 MHz, CD_3OD): δ 173.5, 170.3, 168.9, 158.2, 152.8 (d, *J* = 240.8 Hz), 145.2 (d, *J* = 12.9 Hz), 132.8, 129.3 (d, *J* = 6.0 Hz), 127.6, 126.7 (d, *J* = 3.2 Hz), 118.9 (d, *J* = 3.1 Hz), 118.0 (d, *J* = 18.5 Hz), 116.8, 59.3, 59.2, 40.2, 38.7, 27.4. HRMS (ESI) calcd. for $C_{20}H_{20}FN_2O_5^+$ [(M+H)$^+$] 387.1351, found 387.1354. $[\alpha]_D$: –16.3 (c = 0.75, MeOH, T = 24.5 °C).

UV-Vis spectroscopy

CYP121 and N-terminal His_6–tagged CYP121 proteins were expressed and purified as previously reported.[7a,31] Ligand binding assays were performed by spectrophotometric titration using a Cary 60 UV-visible scanning spectrophotometer (Agilent, UK) and a 1 cm path length quartz cuvette, recording spectra between 250 and 800 nm. Titrations were performed with 3–4 μM protein (CYP121 for analogues **3**–**9** and His_6–tagged-CYP121 for analogues **10**–**18**) at 25 °C

in 100 mM potassium phosphate buffer, 200 mM KCl, pH 7.8. Ligand stock solutions were prepared in DMSO. Ligands were added in small volumes (typically 0.05–0.2 μL aliquots) from concentrated stock solutions to the protein in a 1 mL final volume. Spectral measurements were taken before ligand addition, and following addition of each aliquot of ligand until no further spectral change occurred. Difference spectra at each stage in the titration were obtained by subtraction of the initial ligand-free enzyme spectrum from subsequent spectra collected after each addition of ligand. From the difference spectra, a pair of wavelengths were identified and defined as the absorbance maximum (A_{peak}) and minimum (A_{trough}). The overall absorbance change (ΔA_{max}) was calculated by subtracting the A_{trough} value from the A_{peak} value for each spectrum collected after a ligand addition. Graphs of ΔAmax against [ligand] were plotted for each titration. The K_D values were determined by fitting the data using either a standard hyberbolic function (Equation 1) or the Hill equation (Equation 2) using Origin software (OriginLab, Northampton, MA).

$$A_{obs} = (A_{max} * L/(K_D + L)) \qquad \text{(Equation 1)}$$

In Equation 1 (the standard hyperbolic function), A_{obs} is the observed absorbance change at ligand concentration L, A_{max} is the maximal absorbance change observed at apparent ligand saturation, and K_D is the dissociation constant for the binding of the ligand (the substrate concentration at which $A_{obs} = 0.5 \times A_{max}$).

$$A_{obs} = (A_{max} \times L^n)/(K^n + L^n) \qquad \text{(Equation 2)}$$

In equation 2 (the sigmoidal Hill equation), A_{obs} is the observed absorbance change at ligand concentration L, A_{max} is the absorbance change at apparent ligand saturation, K is the apparent dissociation constant, and n is the Hill coefficient, a value describing the apparent extent of cooperativity observed in ligand binding.

The HS component of each ligand bound to CYP121 was derived from the UV-Vis binding titration spectra and the percentage HS was calculated from the absorbance values for LS and HS CYP121 at 415 and 393 nm using equation 3 (adapted from ref 46.)

$$\% HS = \frac{\varepsilon^{LS}_{415} A_{393} - \varepsilon^{LS}_{393} A_{415}}{A_{393}\left(\varepsilon^{LS}_{415} - \varepsilon^{HS}_{415}\right) - A_{415}\left(\varepsilon^{LS}_{393} - \varepsilon^{HS}_{393}\right)} x\ 100 \qquad \text{(Equation 3)}$$

In equation 3 (calculation of percentage HS for CYP121) A_{393} and A_{415} are absorbance values at Soret maxima for LS and HS species at 415 and 393 nm, respectively. Molar extinction coefficients (ε): ε^{LS}_{415} = 95.00 $mM^{-1}cm^{-1}$, ε^{LS}_{393} = 59.50 $mM^{-1}cm^{-1}$, ε^{HS}_{415} = 60.45 $mM^{-1}cm^{-1}$, ε^{HS}_{393} = 93.86 $mM^{-1}cm^{-1}$ were determined from native CYP121 (LS) and CYP121 bound to compound 9 (HS).

EPR spectroscopy

EPR was performed on a Bruker ELEXSYS E500 spectrometer operating at X-band employing a Super High Q cylindrical cavity (Q factor ~20,000) equipped with an Oxford Instruments ESR900 liquid helium cryostat linked to an ITC503 temperature controller. Spectra were collected at 10K using 0.5 mW microwave power, 100 KHz modulation frequency and 0.7 mT modulation amplitude.

Protein samples (155 μM, CYP121 for analogues **3**–**9** and His_6–tagged-CYP121 for analogues **10**–**18**) were prepared in 100 mM HEPES, 100 mM KCl pH 7.5. Ligand or DMSO were added to a final concentration of 0.5–2 mM depending on solubility. Samples were incubated for 20 min at room temperature and centrifuged briefly to remove any particulate matter prior to transfer to EPR

tubes and freezing in liquid nitrogen. EPR spectra were integrated with reference to a copper sulfate standard to calculate relative concentrations of HS species for each sample.

Crystallography

CYP121A1 protein and crystals were prepared as previously reported,[7] with the following adaptations. Crystals were prepared using a Mosquito pipetting robot (Molecular Dimensions, Newmarket, UK) in 800 nL drops with protein-to-mother liquor at a ratio of 1:1, by vapor diffusion in 1.5–2.1 M ammonium sulfate and 0.1 M sodium MES or Cacodylate from pH 5.5–6.15. Soaked crystals were prepared following incubation with 2 mM ligand prepared in DMSO. Protein solutions were centrifuged at 14,000 rpm for 20 mins at 4 °C immediately before crystallogenesis. Ligand soaks were also carried out either by directly dissolving solid ligand to saturation or by the addition of a 2–5 mM ligand solution in DMSO to the mother liquor, and soaking was carried out for a minimum period of 24 h. Crystals were immersed in mother liquor supplemented with 10–30% oil as cryoprotectant, and cryoprotected and flash-cooled in liquid nitrogen. Data were collected on beamline i02 (wavelength 0.9795 Å) and I24 (wavelength 0.9173/1.0118 Å) at the Diamond Light Source Facility (Harwell, UK). The diffraction data were reduced, scaled and merged using XDS.[47,48] Structures were refined using PHENIX software suite[49] with the native CYP121A1 structure (PDB 1N40)[50] as the starting model. Structural rebuilding and validation were performed with *Coot*,[51] Molprobity[52] and *PDB_REDO*.[53] Data collection and final refinement statistics are provided in the Supplementary Information (Tables S1 and S2). Images for presentation were rendered using an academic version of the PyMOL Molecular Graphics System, Schrödinger, LLC.

Minimum inhibitory concentration (MIC) assays

The compounds were serially diluted (1:2 dilutions) in 96 well plates (0.1% DMSO in TDW). Starting concentrations of these compounds were usually 100 μM and used at a final volume of 10 μl. Rifampicin was used as the positive control. *Mtb* H37Rv was grown to an OD of 0.6–0.8 in 7H9 medium supplemented with ADC enrichment and then, on the day of the assay, the culture was diluted to an OD_{600} of 0.001 and 90 μL of bacterial suspension were added to the compounds. The plate was incubated for 7 days at 37°C. Resazurin [10 μL; 0.05% w/v)] was then added and incubated for 24 h at 37°C, and fluorescence was measured at 590 nm. After subtraction of background fluorescence from all wells, the percentage mycobacterial survival was determined by comparing the fluorescence of wells containing compounds with control wells not treated with compound.

Supporting Information: UV-Vis spectra, EPR spectra, K_D determinations, data collection and refinement statistics of CYP121 in complex with ligands, electron density plots of ligands bound to CYP121, ^{1}H and ^{13}C NMR spectra of compounds **3**–**18** and molecular formula strings (MFS) for compounds **3**–**18**, **22**, **23**, **25a**–**e** are available free of charge on the ACS Publications website at doi: 10.1021/acs.jmedchem.xxxxxxx.

PDB ID Codes: PDB codes for compounds **5**, **11**–**18** bound to CYP121 are 6RQ9, 6RQ8, 6RQB, 6RQD, 6RQ6, 6RQ0, 6RQ5, 6RQ1, 6RQ3, respectively. Authors will release the atomic coordinates and experimental data upon article publication.

AUTHOR INFORMATION

Corresponding Author: Email: chutton@unimelb.edu.au

ORCID

Craig A. Hutton: 0000-0002-2353-9258

Andrew W. Munro: 0000-0002-4642-180X

ACKNOWLEDGMENT

This work was supported by the Australian Research Council (DP180101804 and DP140100174), The University of Melbourne (Manchester–Melbourne Research Fund), and by the UK Biotechnology and Biological Sciences Research Council (BBSRC grant award number BB/R009961/1). The authors also wish to thank the BBSRC-funded Centre for Synthetic Biology of Fine and Specialty Chemicals (SYNBIOCHEM, BB/M017702/1) for access to analytical equipment. We acknowledge Diamond Light Source for time on beamline i03 under proposals

MX8997-25 and MX17773-10 and thank the beamline scientists for their assistance with crystallographic data collection. We thank Dr Nick Williamson and the Bio21 MSPF for their assistance with compound purification and characterization.

ABBREVIATIONS

CYP, cytochrome P450 enzyme; DKP, 2,5-diketopiperazine; DMSO, dimethylsulfoxide; HBTU, *N,N,N′,N′*-tetramethyl-*O*-(1*H*-benzotriazol-1-yl)uronium hexafluorophosphate; HOBt, N-hydroxybenzotriazole; Mtb, *Mycobacterium tuberculosis*; TDW, triple-distilled water.

REFERENCES

(1) Fair, R. J.; Tor, Y. Antibiotics and Bacterial Resistance in the 21st Century. *Perspect. Medicin. Chem.* **2014**, *6*, 25–64.

(2) Kapoor, G.; Saigal, S.; Elongavan, A. Action and Resistance Mechanisms of Antibiotics: a Guide for Clinicians. *J. Anaesthesiol. Clin. Pharmacol.* **2017**, *33*, 300–305.

(3) Gould, K. Antibiotics: From Prehistory to the Present Day. *J. Antimicrob. Chemother.* **2016**, *71*, 572–575.

(4) Cole, S. T.; Brosch, R.; Parkhill, J.; Garnier, T.; Churcher, C.; Harris, D.; Gordon, S. V.; Eiglmeier, K.; Gas, S.; Barry, C. E.; Tekaia, F.; Badcock, K.; Basham, D.; Brown, D.; Chillingworth, T.; Connor, R.; Davies, R.; Devlin, K.; Feltwell, T.; Gentles, S.; Hamlin, N.; Holroyd, S.; Hornsby, T.; Jagels, K.; Krogh, A.; Mclean, J.; Moule, S.; Murphy, L.; Oliver, K.; Osborne, J.; Quail, M. A.; Rajandream, M. A.; Rogers, J.; Rutter, S.; Seeger, K.; Skelton, J.; Squares, R.; Squares, S.; Sulston, J. E.; Taylor, K.; Whitehead, S.;

Barrell, B. G. Deciphering the Biology of *Mycobacterium tuberculosis* from the Complete Genome Sequence. *Nature* **1998**, *393*, 537–544.

(5) Sassetti, C. M.; Boyd, D. H.; Rubin, E. J. Comprehensive Identification of Conditionally Essential Genes in Mycobacteria. *Proc. Natl. Acad. Sci. U.S.A.* **2001**, *98*, 12712–12717.

(6) Sassetti, C. M.; Boyd, D. H.; Rubin, E. J. Genes Required for Mycobacterial Growth Defined by High Density Mutagenesis. *Mol. Microbiol.* **2003**, *48*, 77–84.

(7) (a) Mclean, K. J.; Carroll, P.; Lewis, D. G.; Dunford, A. J.; Seward, H. E.; Neeli, R.; Cheesman, M. R.; Marsollier, L.; Douglas, P.; Smith, W. E.; Rosenkrands, I.; Cole, S. T.; Leys, D.; Parish, T.; Munro, A. W. Characterization of Active Site Structure in CYP121. *J. Biol. Chem.* **2008**, *283*, 33406–33416. (b) Mclean, K. J.; Dunford, A. J.; Sabri, M.; Neeli, R.; Girvan, H. M.; Balding, P. R.; Leys, D.; Seward, H. E.; Marshall, K. R.; Munro, A. W. CYP121, CYP51 and Associated Redox Systems in *Mycobacterium tuberculosis*: Towards Deconvoluting Enzymology of P450 Systems in a Human Pathogen. *Biochem. Soc. Trans.* **2006**, *34*, 1178–1182. (c) Mclean, K. J.; Cheesman, M. R.; Rivers, S. L.; Richmond, A.; Leys, D.; Chapman, S. K.; Reid, G. A.; Price, N. C.; Kelly, S. M.; Clarkson, J.; Smith, W. E.; Munro, A. W. Expression, Purification and Spectroscopic Characterization of the Cytochrome P450 CYP121 from *Mycobacterium tuberculosis*. *J. Inorg. Biochem.* **2002**, *91*, 527–541.

(8) (a) Girvan, H. M.; Munro A. W. Applications of Microbial Cytochrome P450 Enzymes in Biotechnology and Synthetic Biology. *Curr Opin Chem Biol*., **2016**, *31*, 136–145. (b) Guengerich F. P.; Munro A. W. Unusual Cytochrome P450 Enzymes and Reactions (2013), *J. Biol. Chem., 2013, 288*,17065–17073.

(9) Belin, P.; Le Du, M. H.; Fielding, A.; Lequin, O.; Jacquet, M.; Charbonnier, J.-B.; Lecoq, A.; Thai, R.; Courçon, M.; Masson, C.; Dugave, C.; Genet, R.; Pernodet, J.-L.; Gondry, M. Identification and Structural Basis of the Reaction Catalyzed by CYP121, an Essential Cytochrome P450 in *Mycobacterium tuberculosis*. *Proc. Natl. Acad. Sci. U.S.A.* **2009**, *106*, 7426–7431.

(10) (a) Zerbe, K.; Pylypenko, O.; Vitali, F.; Zhang, W. W.; Rouse, S.; Heck, M.; Vrijbloed, J. W.; Bischoff, D.; Bister, B.; Sussmuth, R. D.; Pelzer, S.; Wohlleben, W.; Robinson, J. A.; Schlichting, I. Crystal Structure of OxyB, a Cytochrome P450 Implicated in an Oxidative Phenol Coupling Reaction During Vancomycin Biosynthesis. *J. Biol. Chem.* **2002**, *277*, 47476–47485. (b) Pylypenko, O.; Vitali, F.; Zerbe, K.; Robinson, J. A.; Schlichting, I. Crystal Structure of OxyC, a Cytochrome P450 Implicated in an Oxidative Phenol Coupling Reaction During Vancomycin Biosynthesis. *J. Biol. Chem.* **2003**, *278*, 46727–46733. (c) Cryle, M. J.; Staaden, J.; Schlichting, I. Structural Characterization of CYP165D3, a Cytochrome P450 Involved in Phenolic Coupling in Teicoplanin Biosynthesis. *Arch. Biochem. Biophys.* **2011**, *507*,163–173. (d) Li, Z.; Rupasinghe, S. G.; Schuler, M. A.; Nair, S. K. Crystal Structure of a Phenol-coupling P450 Monooxygenase Involved in Teicoplanin Biosynthesis *Proteins* **2011**, *79*, 1728–1738. (e) Peschke, M.; Brieke, C.; Cryle, M. J. F-O-G Ring Formation in Glycopeptide Antibiotic Biosynthesis is Catalysed by OxyE. *Sci Rep.* **2016**, *6*, 35584. (f) Peschke, M.; Gonsior, M.; Süssmuth, R. D.; Cryle, M. J. Understanding the Crucial Interactions Between Cytochrome P450s and Non-Ribosomal Peptide Synthetases During Glycopeptide Antibiotic Biosynthesis. *Curr. Opin. Struct. Biol.* **2016**, *41*, 46–53.

(11) Mclean, K. J.; Marshall, K. R.; Richmond, A.; Hunter, I. S.; Fowler, K.; Kieser, T.; Gurcha, S. S.; Besra, G. S.; Munro, A. W. Azole Antifungals are Potent Inhibitors of Cytochrome P450 Mono-Oxygenases and Bacterial Growth in Mycobacteria and Streptomycetes. *Microbiol.* **2002**, *148*, 2937–2949.

(12) Sundaramurthi, J. C.; Kumar, S.; Silambuchelvi, K.; Hanna, L. E. Molecular Docking of Azole Drugs and their Analogs on CYP121 of *Mycobacterium tuberculosis*. *Bioinformation* **2011**, *7*, 130–133.

(13) Mast, N.; Zheng, W.; Stout, C. D.; Pikuleva, I. A. Antifungal Azoles: Structural Insights into Undesired Tight Binding to Cholesterol-Metabolizing CYP46A1. *Mol. Pharmacol.* **2013**, *84*, 86–94.

(14) Martins, M. B.; Carvalho, I. Diketopiperazines: Biological Activity and Synthesis. *Tetrahedron* **2007**, *63*, 9923–9932.

(15) Omura, S.; Hirano, A.; Iwai, Y.; Masuma, R. Herquline, A New Alkaloid Produced by *Penicillium herquei*. Fermentation, Isolation and Properties. *J. Antibiot.* **1979**, *32*, 786–790.

(16) Enomoto, Y.; Shiomi, K.; Hayashi, M.; Masuma, R.; Kawakubo, T.; Tomosawa, K.; Iwai, Y.; Omura, S. Herquline B, A Newplatelet Aggregation Inhibitor Produced by *Penicillium herquei* Fg-372. *J. Antibiot.* **1996**, *49*, 50–53.

(17) Furusaki, A.; Matsumoto, T.; Ogura, H.; Takayanagi, H.; Hirano, A.; Omura, S. X-Ray Crystal Structure of Herquline, a New Biologically Active Piperazine from *Penicillium herquei* Fg-372. *J. Chem. Soc., Chem. Commun.* **1980**, 698.

(18) Zhu, X.; Mcatee, C. C.; Schindler, C. S. Total Syntheses of Herqulines B and C. *J. Am. Chem. Soc.* **2019**, *141*, 3409–3413.

(19) He, C.; Stratton, T. P.; Baran, P. S. Concise Total Synthesis of Herqulines B and C. *J. Am. Chem. Soc.* **2019**, *141*, 29–32.

(20) Cox, J. B.; Kimishima, A.; Wood, J. L. Total Synthesis of Herquline B and C. *J. Am. Chem. Soc.* **2019**, *141*, 25–28.

(21) Nishiyama, S.; Nakamura, K.; Suzuki, Y.; Yamamura, S. Synthesis of Piperazinomycin, a Novel Antifungal Antibiotic. *Tetrahedron Lett.* **1986**, *27*, 4481–4484.

(22) Tamai, S.; Kaneda, M.; Nakamura, S. Synthesis Of Piperazinomycin, A Novel Antifungal Antibiotic. I. Fermentation, Isolation, Characterization and Biological Properties. *J. Antibiot.* **1982**, *35*, 1130–1136.

(23) Boger, D. L.; Zhou, J. Total Synthesis of (+)-Piperazinomycin. *J. Am. Chem. Soc.* **1993**, *115*, 11426–11433.

(24) Cochrane, J. R.; White, J. M.; Wille, U.; Hutton, C. A. Total Synthesis of Mycocyclosin. *Org. Lett.* **2012**, *14*, 2402–2405.

(25) Zhu, X.; Mcatee, C. C.; Schindler, C. S. Scalable Synthesis of Mycocyclosin. *Org. Lett.* **2018**, *20*, 2862–2866.

(26) Fonvielle, M.; Le Du, M. H.; Lequin, O.; Lecoq, A.; Jacquet, M.; Thai, R.; Dubois, S.; Grach, G.; Gondry, M.; Belin, P. Substrate and Reaction Specificity of *Mycobacterium*

tuberculosis Cytochrome P450 CYP121. Insights from Biochemical Studies and Crystal Structures. *J. Biol. Chem.* **2013**, *288*, 17347–17359.

(27) Kavanagh, M. E.; Coyne, A. G.; Mclean, K. J.; James, G. G.; Levy, C. W.; Marino, L. B.; De Carvalho, L. P. S.; Chan, D. S. H.; Hudson, S. A.; Surade, S.; Leys, D.; Munro, A. W.; Abell, C. Fragment-Based Approaches to the Development of *Mycobacterium tuberculosis* CYP121 Inhibitors. *J. Med. Chem.* **2016**, *59*, 3272–3302.

(28) Duffell, K. M.; Hudson, S. A.; Mclean, K. J.; Munro, A. W.; Abell, C.; Matak-Vinković, D. Nanoelectrospray Ionization Mass Spectrometric Study of *Mycobacterium tuberculosis* CYP121−Ligand Interactions. *Anal. Chem.* **2013**, *85*, 5707–5714.

(29) Taban, I. M.; Elshihawy, H. E. A. E.; Torun, B.; Zucchini, B.; Williamson, C. J.; Altuwairigi, D.; Ngu, A. S. T.; Mclean, K. J.; Levy, C. W.; Sood, S.; Marino, L. B.; Munro, A. W.; De Carvalho, L. P. S.; Simons, C. Novel Aryl Substituted Pyrazoles as Small Molecule Inhibitors of Cytochrome P450 CYP121A1: Synthesis and Antimycobacterial Evaluation. *J. Med. Chem.* **2017**, *60*, 10257–10267.

(30) Kavanagh, M. E.; Gray, J. L.; Gilbert, S. H.; Coyne, A. G.; Mclean, K. J.; Davis, H. J.; Munro, A. W.; Abell, C. Substrate Fragmentation for the Design of *M. tuberculosis* CYP121 Inhibitors. *Chemmedchem* **2016**, *11*, 1924–1935.

(31) Hudson, S. A.; Mclean, K. J.; Surade, S.; Yang, Y.-Q.; Leys, D.; Ciulli, A.; Munro, A. W.; Abell, C. Application of Fragment Screening and Merging to the Discovery of Inhibitors

of the *Mycobacterium tuberculosis* Cytochrome P450 CYP121. *Angew. Chem. Int. Ed.* **2012**, *51*, 9311–9316.

(32) Marcuccio, S. M.; Elix, J. A. Pyrazine Chemistry. II. Reduction of 3,6-Dibenzylidenepiperazine-2,5-Diones. *Aust. J. Chem.* **1984**, *37*, 1791–1794.

(33) Marcuccio, S. M.; Elix, J. A. Pyrazine Chemistry. V. Synthesis of Methylanhydropicroroccellin and Dimethylpicroroccellin. *Aust. J. Chem.* **1985**, *38*, 1785–1796.

(34) Saito, N.; Harada, S.; Yamashita, M.; Saito, T.; Yamaguchi, K.; Kubo, A. Synthesis of Saframycins. XI. Synthetic Studies Toward a Total Synthesis of Safracin A. *Tetrahedron* **1995**, *51*, 8213–8230.

(35) (a) Chenge, J. T.; Duyet, L. V.; Swami, S.; Mclean, K. J.; Kavanagh, M. E.; Coyne, A. G.; Rigby, S. E. J.; Cheesman, M. R.; Girvan, H. M.; Levy, C. W.; Rupp, B.; Kries, Von, J. P.; Abell, C.; Leys, D.; Munro, A. W. Structural Characterization and Ligand/Inhibitor Identification Provide Functional Insights into the *Mycobacterium tuberculosis* Cytochrome P450 CYP126A1. *J. Biol. Chem.* **2017**, *292*, 1310–1329. (b) Mclean, K. J.; Warman, A. J.; Seward, H. E.; Marshall, K. R.; Girvan, H. M.; Cheesman, M. R.; Waterman, M. R.; Munro, A. W. Biophysical Characterization of the Sterol Demethylase P450 from *Mycobacterium tuberculosis*, its Cognate Ferredoxin, and their Interactions. *Biochemistry* **2006**, *45*, 8427–8443.

(36) Alkhalaf, L. M.; Barry, S. M.; Rea, D.; Gallo, A.; Griffiths, D.; Lewandowski, J. R.; Fulop, V.; Challis, G. L. Binding of Distinct Substrate Conformations Enables Hydroxylation of Remote Sites in Thaxtomin D by Cytochrome P450 TxtC *J. Am. Chem. Soc.* **2019**, *141*, 216–222.

(37) Brookhart, M.; Green, M. L. H.; Parkin, G. Agostic Interactions in Transition Metal Compounds. *Proc. Natl. Acad. Sci. U.S.A.* **2007**, *104*, 6908–6914.

(38) Yu, M.; Nagalingam, G.; Ellis, S.; Martinez, E.; Sintchenko, V.; Spain, M.; Rutledge, P. J.; Todd, M. H.; Triccas, J. A. Nontoxic Metal−Cyclam Complexes, a New Class of Compounds with Potency Against Drug-Resistant *Mycobacterium tuberculosis*. *J. Med. Chem.* **2016**, *59*, 5917–5921.

(39) Mast, N.; Zheng, W.; Stout, C. D.; Pikuleva, I. A. Binding of a Cyano- and Fluoro-Containing Drug Bicalutamide to Cytochrome P450 46A1: Unusual Features And Spectral Response. *J. Biol. Chem.* **2013**, *288*, 4613–4624.

(40) (a) Politzer, P.; Murray, J. S.; Clark, T. Halogen Bonding and other σ-Hole Interactions: A Perspective. *Phys. Chem. Chem. Phys.* **2013**, *15*, 11178–11189. (b) Mondal, S.; Gong, X.; Zhang, X.; Salinger, A. J.; Zheng, L.; Sen, S.; Weerapana, E.; Zhang, X.; Thompson, P. R. Halogen Bonding Increases the Potency and Isozyme Selectivity of Protein Arginine Deiminase 1 Inhibitors. *Angew. Chem. Int. Ed.* **2019**, *58*, 1–6.

(41) Huang, Z.; Yang, R.; Guo, Z.; She, Z.; Lin, Y. A New Xanthone Derivative from Mangrove Endophytic Fungus No. ZSU-H16. *Chem. Nat. Compd.* **2010**, *46*, 348–351.

(42) Lu, X.; Shen, Y.; Zhu, Y.; Xu, Q.; Liu, X.; Ni, K.; Cao, X.; Zhang, W.; Jiao, B. Diketopiperazine Constituents of Marine *Bacillus Subtilis*. *Chem. Nat. Compd.* **2009**, *45*, 290–292.

(43) Rosenmund, P.; Kaiser, K. Diketopiperazines from Leuchs Anhydrides. *Angew. Chem. Int. Ed. Engl.* **1970**, *9*, 162–163.

(44) Bérubé, C.; Barbeau, X.; Cardinal, S.; Boudreault, P.-L.; Bouchard, C.; Delcey, N.; Lagüe, P.; Voyer, N. Interfacial Supramolecular Biomimetic Epoxidation Catalysed by Cyclic Dipeptides. *Supramol. Chem.* **2017**, *29*, 330–349.

(45) Jung, M. E.; Rohloff, J. C. Organic Chemistry of L-Tyrosine. 1. General Synthesis of Chiral Piperazines from Amino Acids. *J. Org. Chem.* **1985**, *50*, 4909–4913.

(46) Tran, N.-H.; Huynh, N.; Chavez, G.; Nguyen, A.; Dwaraknath, S.; Nguyen, T.-A.; Nguyen, M.; Cheruzel, L. A Series of Hybrid P450 BM3 Enzymes with Different Catalytic Activity in the Light-Initiated Hydroxylation of Lauric Acid. *J. Inorg. Biochem.* **2012**, 115, 50–56.

(47) Kabsch, W. XDS. *Acta Crystallogr. D Biol. Crystallogr.* **2010**, *66*, 125–132.

(48) Winter, G. Xia2: An Expert System for MX Data Reduction. *J. Appl. Crystallogr.* **2009**, *43*, 186–190.

(49) Adams, P. D.; Afonine, P. V.; Bunkóczi, G.; Chen, V. B.; Davis, I. W.; Echols, N.; Headd, J. J.; Hung, L.-W.; Kapral, G. J.; Grosse-Kunstleve, R. W.; Mccoy, A. J.; Moriarty, N. W.; Oeffner, R.; Read, R. J.; Richardson, D. C.; Richardson, J. S.; Terwilliger, T. C.; Zwart, P. H. PHENIX: A Comprehensive Python-Based System for Macromolecular Structure Solution. *Acta Crystallogr. D Biol. Crystallogr.* **2010**, *66*, 213–221.

(50) Leys, D.; Mowat, C. G.; Mclean, K. J.; Richmond, A.; Chapman, S. K.; Walkinshaw, M. D.; Munro, A. W. Atomic Structure of *Mycobacterium tuberculosis* CYP121 to 1.06 Å Reveals Novel Features of Cytochrome P450. *J. Biol. Chem.* **2003**, *278*, 5141–5147.

(51) Emsley, P.; Lohkamp, B.; Scott, W. G.; Cowtan, K. Features and Development of *Coot*. *Acta Crystallogr. D Biol. Crystallogr.* **2010**, *66*, 486–501.

(52) Chen, V. B.; Arendall, W. B.; Headd, J. J.; Keedy, D. A.; Immormino, R. M.; Kapral, G. J.; Murray, L. W.; Richardson, J. S.; Richardson, D. C. Molprobity: All-Atom Structure Validation for Macromolecular Crystallography. *Acta Crystallogr. D Biol. Crystallogr.* **2010**, *66*, 12–21.

(53) Joosten, R. P.; Long, F.; Murshudov, G. N.; Perrakis, A. The PDB_REDO Server for Macromolecular Structure Model Optimization. *IUCRJ* **2014**, *1*, 213–220.

Table of Contents graphic